Photogrammetric Determination of Surface Altitude, Terminus Position, and Ice Velocity of Columbia Glacier, Alaska

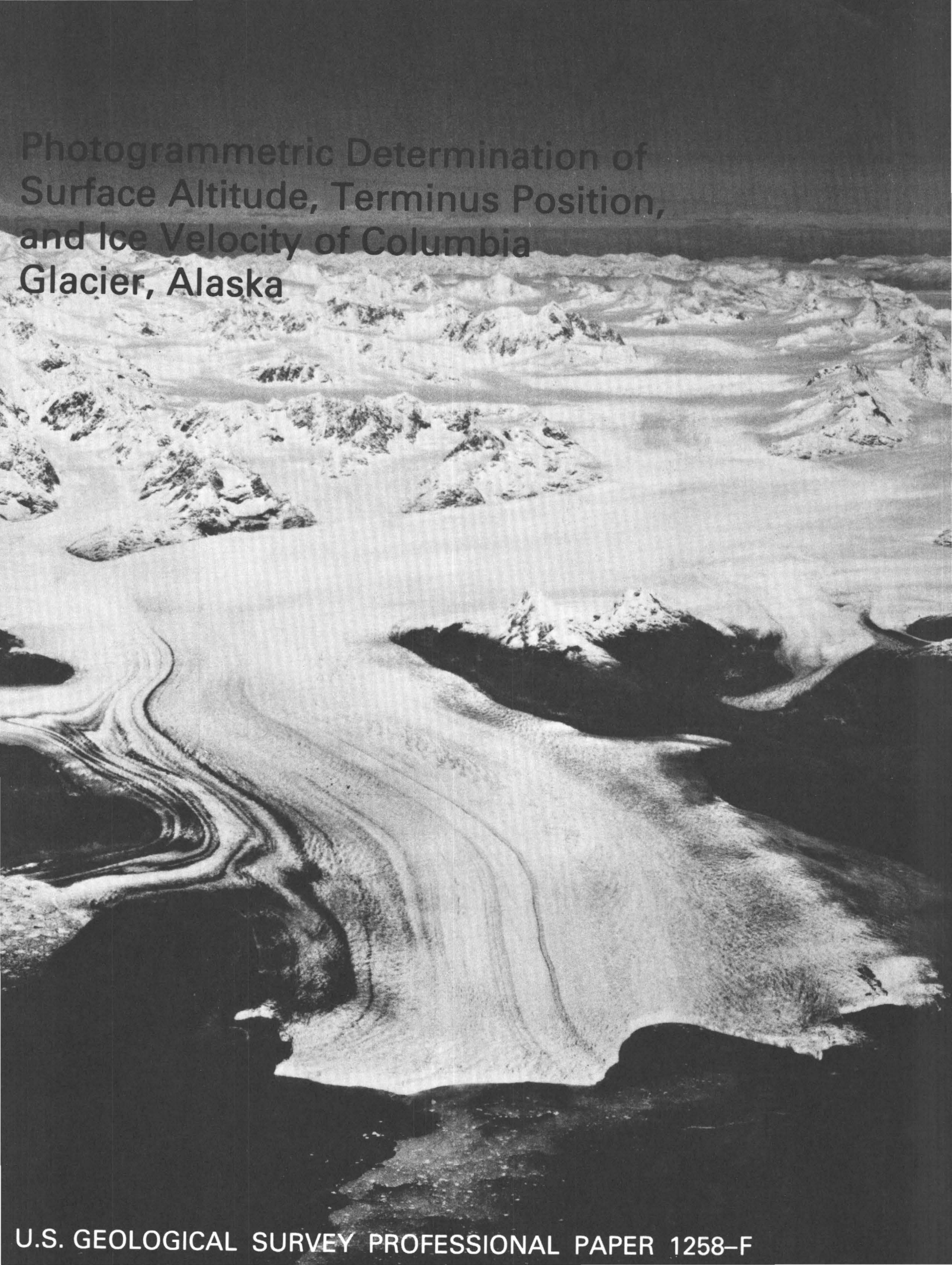

U.S. GEOLOGICAL SURVEY PROFESSIONAL PAPER 1258–F

Photogrammetric Determination of Surface Altitude, Terminus Position, and Ice Velocity of Columbia Glacier, Alaska

By M. F. MEIER, L. A. RASMUSSEN, R. M. KRIMMEL, R. W. OLSEN *and* DAVID FRANK

STUDIES OF COLUMBIA GLACIER, ALASKA'

U.S. GEOLOGICAL SURVEY PROFESSIONAL PAPER 1258–F

Digital photogrammetric methods are used to determine how the pattern of retreat, thinning, and flow changes through time, and how the flow reacts to changes in the terminus of this iceberg-calving glacier

UNITED STATES GOVERNMENT PRINTING OFFICE, WASHINGTON : 1985

DEPARTMENT OF THE INTERIOR

DONALD PAUL HODEL, *Secretary*

U.S. GEOLOGICAL SURVEY

Dallas L. Peck, *Director*

Library of Congress Cataloging in Publication Data
Main entry under title:

Photogrammetric determination of surface altitude, terminus position, and ice velocity of Columbia Glacier, Alaska.

(Studies of Columbia Glacier, Alaska) (Geological Survey professional paper ; 1258-F)
Bibliography: p.
Supt. of Docs. no.: I 19.16:1258-F
1. Columbia Glacier (Alaska) I. Meier, Mark Frederick, 1925- . II. Series. III. Series: Geological Survey professional paper ; 1258-F.
GB2427.C64P47 1985 551.3'12'097983 84-600196

For sale by the Distribution Branch, U.S. Geological Survey
604 South Pickett Street, Alexandria, VA 22304

CONTENTS

ILLUSTRATIONS

[Plates are in pocket]

TABLES

SYMBOLS AND ABBREVIATIONS

Symbol	Name	Units (where applicable)
a	Year.	----------
b	Subscript denoting basal sliding.	----------
c	Subscript denoting calving.	----------
D	Number of days after January 1, 1978 -----	days
d	Subscript denoting deformation.	----------
e	Subscript denoting terminus.	----------
g	Function giving v_ξ in terms of ξ ----------	km/a
h	Glacier thickness ----------	m
i	Row index of square grid.	----------
j	Column index of square grid.	----------
km	Kilometer.	----------
L	Subscript denoting flight number.	----------
m	Meter.	----------
n	Flow law exponent ----------	dimensionless
r	Function giving $1/v_\xi$ in terms of ξ ----------	a/km
t	Time ----------	a
UTM	Universal Transverse Mercator.	----------
u	Velocity component in x-direction ----------	km/a
$\overline{u}$	Measurement-year average of u ----------	km/a
v	Velocity component in y-direction ----------	km/a
$\overline{v}$	Measurement-year average of v ----------	km/a
v_ξ	Velocity component in ξ-direction ----------	km/a
$\hat{V}$	Maximum value of $\lvert v \rvert$ in a particular row ---	km/a
$\overline{V}$	Long-term average of V(June 2, 1977, September 1, 1981) ----------	km/a
$\hat{V}$	Normalized velocity $V/\overline{V}$ ----------	dimensionless
V_b	Sliding part of V ----------	km/a
$\langle V_c \rangle$	Width-averaged calving velocity ----------	km/a
V_d	Deformational part of V ----------	km/a
$\langle V_e \rangle$	Width-averaged velocity at terminus ------	km/a
x	Horizontal coordinate, positive to east -----	km
y	Horizontal coordinate, positive to north	km
Y	Point on pseudo-trajectory ----------	km
Z	Glacier surface altitude ----------	m
α	Slope of glacier surface ----------	dimensionless
Δ	Grid spacing (0.7625 km) ----------	km
$\dot{\epsilon}$	Component of strain rate tensor ----------	a^{-1}
λ	Ratio of sliding velocity to total velocity ----	dimensionless
μm	Micrometer.	----------
θ	Angle between principal component of $\dot{\epsilon}$ and ξ-axis ----------	degrees
Ξ	Terminus position, measured in ξ-direction --	km
$\langle \Xi \rangle$	Width-averaged terminus position, measured in ξ-direction ----------	km
ξ	Curvilinear coordinate, parallel to glacier centerline ----------	km
ζ	Curvilinear coordinate, normal to ξ-direction	km

Note: Use of firm names or their products in this report is for identification purposes only and does not constitute endorsement by the U.S. Geological Survey.

PHOTOGRAMMETRIC DETERMINATION OF SURFACE ALTITUDE, TERMINUS POSITION, AND ICE VELOCITY OF COLUMBIA GLACIER, ALASKA

By M. F. MEIER, L. A. RASMUSSEN, R. M. KRIMMEL, R. W. OLSEN, and DAVID FRANK

ABSTRACT

More than 6,000 location and velocity measurements were made on Columbia Glacier, using modern digital photogrammetric instruments, from vertical aerial photographs taken during 30 aerial photographic survey flights. A simple photograph-overlay method was used to obtain additional data. Maps of the surface topography of the lower reach of Columbia Glacier were constructed from 1957, 1974, 1977, 1978, and 1981 photographic surveys. During this period, the glacier thinned. The terminus exhibited a seasonal cycle of winter advance and summer retreat superimposed on a longer term accelerating retreat. During 1977–79, embayments formed each summer and fall and closed each winter and spring.

The surface-velocity pattern resembles that of an ice stream in an ice sheet: the main trunk glacier flows as a discrete, high-velocity (~1 kilometer per year) stream through a maze of relatively slowly moving tributaries. In one reach, longitudinal normal strain rates exceed two per year in extension and one per year in compression. Although flow in the lower reach is very fast (0.8 to 2 kilometers per year), no abrupt shear occurs along the margins. Velocity changes with time and distance show a seasonal acceleration and deceleration that is synchronous along the length of the lower reach, peaking in late April; this acceleration and deceleration must be due to changing water pressure at the bed. In addition, a seasonal pulse of high velocity at the terminus occurs in November; it propagates and diffuses upglacier. This pulse is caused by seasonal retreat of the terminus.

INTRODUCTION

Nearly all grounded, iceberg-calving glaciers in Alaska have experienced large-scale, asynchronous advances and retreats. This behavior apparently is not directly related to climatic variations. A critical factor appears to be the water depth at the terminus; instability results when a calving glacier retreats from a moraine shoal into a deep fjord or basin. The glacier may then retreat rapidly and irreversibly as the rate of calving of icebergs increases and unusual volumes of ice break off and float away (Post, 1975).

Columbia Glacier, near Valdez, Alaska (fig. 1), is a large calving glacier; it is 67 km long and 1,100 km^2 in area. The glacier ended in shallow water a short distance behind the crest of a moraine shoal during the period 1974 to 1980, but 5 km upglacier from the terminus the bed is about 400 m below sea level. The glacier is grounded throughout, except for some small areas associated with glacier-dammed lakes; none of the tidewater terminus is floating. Although the position of the terminus has been nearly stationary since it was first mapped in 1794 (Vancouver, 1798), evidence now suggests that rapid, drastic retreat may be imminent (Post, 1975). Small icebergs drift from Columbia Glacier toward, and occasionally into, Valdez Arm. The shoal arrests the progress of icebergs that draw more than about 25 m. Drastic retreat would increase substantially the discharge of ice and might thus increase the iceberg hazard to shipping. To determine when this might happen and how much the iceberg discharge might increase, an intensive study was begun by the U.S. Geological Survey in 1977, and a preliminary prediction was issued in 1980 (Meier and others, 1980).

The scientific results of this study are being published in a series of papers, of which this paper is a part. The other papers in the series discuss the relationship of calving speed to water depth and other variables (Brown and others, 1982); surface topography (Rasmussen and Meier, 1984); mass-balance observations; field measurements of velocity, thickness, and thickness change; development of a data set that satisfies the continuity equation; a continuity model of the terminus

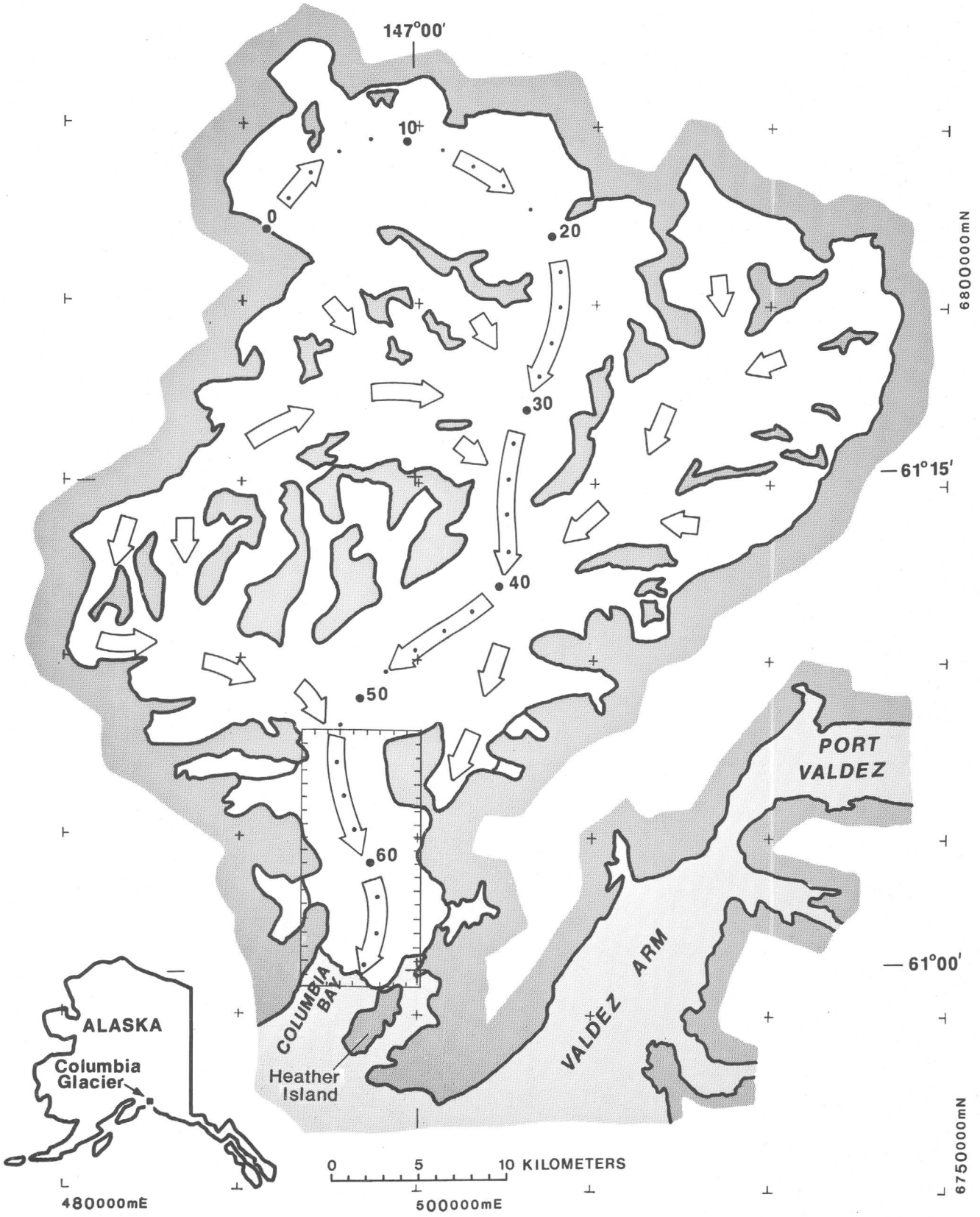

FIGURE 1.—Columbia Glacier, Alaska. Arrows show the direction of flow; longer arrows indicate the main ice stream. Dots are at 2-kilometer intervals along the ξ-axis. The box marks the section of the square ($\Delta x = \Delta y = 762.5$ m) data grid consisting of (horizontal) rows 51–71, numbered from north to south, and of (vertical) columns 18–27, numbered from west to east.

retreat and the rate of iceberg discharge (Rasmussen and Meier, 1982); finite-element (Sikonia, 1982) and finite-difference (Bindschadler and Rasmussen, 1983) models of the flow of the lower glacier; and several additional topics.

Development of a predictive model requires knowledge of the rate of iceflow to the terminus of a calving glacier and the rate of ice loss by calving from the terminus. The flow of Columbia Glacier cannot be analyzed as a conventional problem in dynamics because its flow is due largely to basal sliding and also is dependent on the rate of calving at the terminus. Thus, a complete set of velocity data is required for checking the unusual aspects of the flow. Extra velocity values were required for inferring ice thickness where data could not be obtained. Furthermore, modeling requires accurate data in which the velocity field is consistent with the glacier geometry through the equations of continuity and glacier flow. Otherwise, the glacier model would rapidly redistribute the mass of the glacier, not as a valid representation of the glacier's motion but artificially, to compensate for the inconsistencies in the initial conditions. Consequently, it was necessary to define the surface flow field in great detail both in time and in space; about 6,000 velocity measurements were made. In addition, the ice-surface configuration and its changes over time and the changing configuration of the terminus ice cliff had to be measured.

Most of the velocity, surface-altitude, and terminus-position data were obtained by aerial photogrammetry using metric cameras and modern digital photogrammetric instrumentation; the first section describes this methodology. Next, the acquisition of additioal velocity data by simple photograph-overlay methods and by measurement of ogive spacing is explained. Surface altitude and its changes with time are described, and results are given on the changes in terminus configuration and position. The spatial character of the velocity field for the glacier as a whole during the 1977–78 measurement year is then discussed, as is the pattern of strain rate. The extensive measurements of the time changes in the velocity field over the lowest 14 km of the glacier are described next, and these changes are related to embayment formation.

Measurement of glacier flow using photogrammetric methods was pioneered by Finsterwalder (1931). Additional studies have been made in such locations as Washington State (Hofmann, 1952), Spitzbergen (Pillewizer, 1939), the Soviet Union (Kniznikov, 1962), Greenland (Bauer, 1968), and Antarctica (Adler, 1964). The study of Columbia Glacier differs from this earlier work in that it uses modern analytical and digital methods to process large amounts of data and includes the monitoring of changes in the velocity and deformation-rate fields through time. A somewhat similar study of Hays Glacier, Antarctica, and vicinity has been accomplished (S. Meier, 1973; S. Meier and others, 1978). A recent paper by Brecher (1983) reported a high spatial density of velocity and surface-altitude data, obtained by digital photogrammetry of Byrd Glacier, Antarctica.

METHODS OF DATA ACQUISITION

DIGITAL PHOTOGRAMMETRY

The surface of almost all of the lowest 14 km of Columbia Glacier, and of many other reaches upstream, is spectacularly crevassed (figs. 2, 3). Foot travel and even helicopter landings are impossible in many areas, and the surface-deformation rate is very high. Consequently, conventional stake surveys of glacier velocity and surface altitude cannot be made on the lower glacier except at a few fortuitous locations. On the other hand, the situation is ideal for using photogrammetry to measure points on the glacier. The intricate crevasse pattern provides a large number of identifiable points on the surface. The crevassing is so active that winter snowcover does not obliterate the pattern. Thus, it is possible to track the coordinates of numerous points on the glacier surface without placing markers on the ice.

Most of the data used to monitor changes in shape and movement of Columbia Glacier were acquired photogrammetrically; that is, ground features in three dimensions were measured by comparing overlapping aerial photographs. Three primary phases of photogrammetric data acquisition are (a) planning for and obtaining aerial photographs, (b) referring the photographs to known control points, and (c) digitizing points on the glacier surface and transforming them into horizontal coordinates and altitudes (Slama and others, 1980). At intervals of 1 to 4 months, a new set of aerial photographs is acquired and the procedure is repeated. Most of the photogrammetric processing for the project was performed at the U.S. Geological Survey's Western Mapping Center in Menlo Park, Calif.

Movement of the glacier is measured by computing the change in the coordinates of surface points between successive dates of aerial photographic surveys. The velocity is approximated by dividing the displacement by the time interval and is assigned to a point midway along the trajectory. This "trajectory-average" method normally suffices because the strain rates and the time intervals generally are small, but in some areas a more complex analysis (Rasmussen, 1983) is used.

AERIAL PHOTOGRAPHY AND FIELD CONTROL

Aerial photography is planned in accordance with photogrammetric requirements. The flight plan makes

FIGURE 2.—Oblique aerial photograph showing roughness of the glacier surface. The major crevasse valleys are about 20 m deep and 50 m apart. The center of the scene is about 2.5 km upglacier from the terminus, view to southeast. The glacier flows from left to right. U.S. Geological Survey photograph No. 75M5–56, by L. R. Mayo, October 8, 1975.

it necessary to use a calibrated aerial-mapping camera having a low-distortion, 150-millimeter focal length, wide-angle lens and a 23-centimeter-square photograph format. A single flight line is required, one alined with the glacier so that each photograph taken includes bare ground on each side of the glacier (figs. 4, 5). A nominal flying height of 7,000 m above the average terrain satisfies this requirement, providing a nominal photograph scale of 1:46,000. The flight plan also specifies a maximum distance between exposures so that every part of the glacier is covered by at least two successive photographs to provide stereoscopic coverage for three-dimensional measurement. The typical flight plan shown in figure 5 was used for almost all flights.

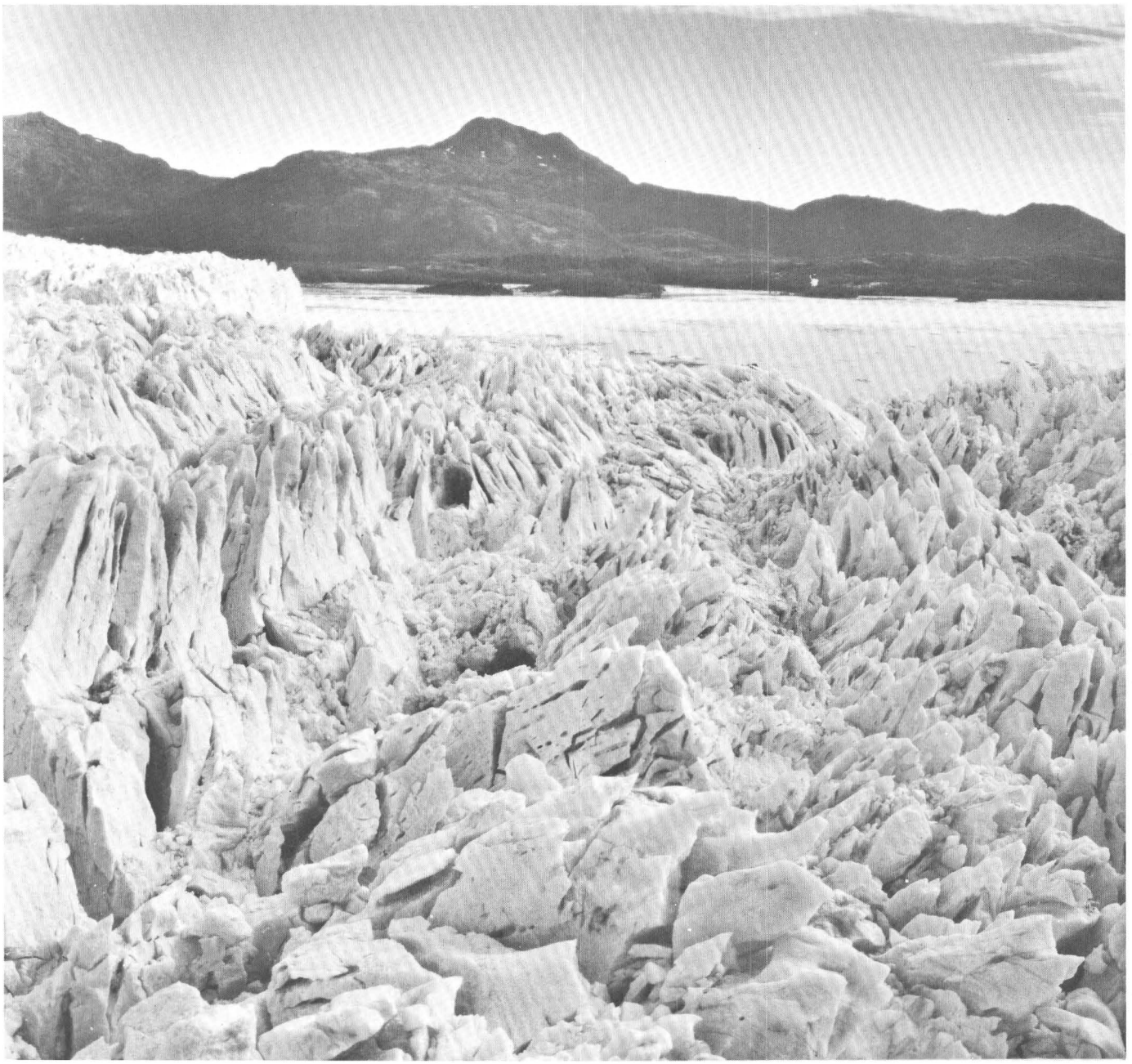

FIGURE 3.—Low-altitude oblique aerial photograph showing detail of the intensely fractured ice surface. This photograph shows an area about 1 km from the terminus and about 1 km from the west margin, view to south-southeast. Flow is diagonal to the right and away from the camera. U.S. Geological Survey photograph No. 75M5–62, by L. R. Mayo, October 8, 1975.

Control is obtained by referring each set of aerial photographs to a consistent ground datum. A combination of sparse field geodetic surveys and photogrammetric control extension, called aerotriangulation, is used. Initially, ground control points were surveyed in the field using geodetic triangulation and distance measurement (M. F. Meier and others, 1978; Mayo and others, 1979). Because of the high cost of field measurements, the number of points was kept low. The field control points, located on bare ground close enough to the glacier to be covered by the aerial photographs, are shown in figure 5. In addition, each point was identified during one or another of the flights by placing white or black panels on the ground surrounding the point.

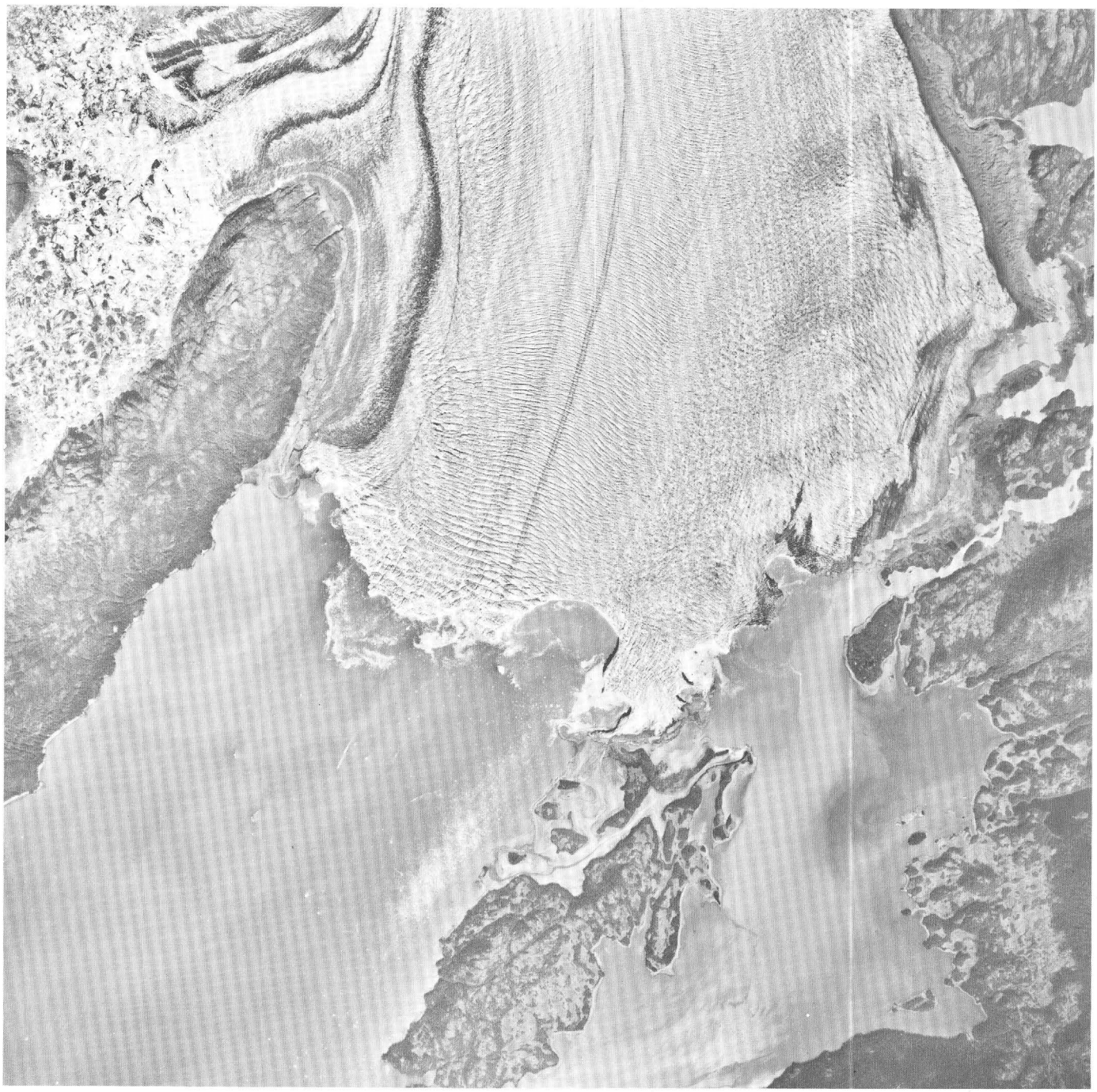

FIGURE 4.—Vertical aerial photograph from about 7,000 m above sea level showing terminus, including a large embayment toward the east edge, and the lowest 6 km of the lower reach, August 26, 1978. North is to the top.

Digital photogrammetric techniques were used to transfer the control point locations from these photographs onto photographs taken at other times.

AEROTRIANGULATION

Aerotriangulation is used to bridge between ground control points for coordinate determination of any point on the ground or the glacier that is measurable on the photographs. The geometry of overlappiong aerial photographs forms the basis for the mathematical transformation. Aerotriangulation involves (1) point selection and marking on the diapositives, (2) measurement with a precision comparator, and (3) computational adjustment of data to generate coordinates.

Control points, photogrammetric passpoints, and desired points on the glacier are used. Control point loca-

tions are transferred onto subsequent sets of aerial photographs by using a precision photogrammetric-point-transfer device that is accurate to within 20 μm on the photographs. Passpoints are required for the mathematical adjustment and are located within the triple overlap areas of the photographs to bridge between successive pairs of photographs along the flight line. Points on the glacier and along the terminus are selected according to a specified grid. Each point is marked by drilling a 30 μm hole into the emulsion of the diapositive and is assigned a unique number.

The measurement is done with a digitizing stereocomparator to obtain a set of x–y image coordinates for points in each of two overlapping photographs. A floating mark is used by the operator to determine a point at the apparent surface of the ice or ground, effecting a measurement of altitude as the computer is used to recreate the third dimension.

The mathematical adjustment corrects systematic errors in the photography, including lens and film distortion, refraction, and Earth curvature. For each overlapping pair of photographs, the corrected image coordinates are used to form an analytical three-dimensional "model." The proper orientation of the photographs in space is that which provides straight lines from camera to image point to ground for every measured point. Next, the models are joined to adjacent models by using common passpoints, and all models are transformed to ground coordinates by using control-point coordinates. The computer program that performs the transformation model-to-model and model-to-ground uses a three-dimensional linear coordinate transformation arising from a least squares adjustment of redundant data (Olsen, 1975). The redundancy produces residuals, which are used to isolate the correct errors and to estimate the accuracy of computed coordinates. The results identify horizontal coordinates and altitudes for all measured points.

ACCURACY OF MEASUREMENT

The photogrammetric accuracy for well-defined points is about 2 m for both the horizontal and vertical coordinates; thus, the measurement accuracy of a horizontal displacement vector from one time to the next is about $2\sqrt{2} \sim 3$ m. However, the horizontal component of ablation in the 1- to 4-month interval between survey flights may add an error, generally not larger than 1–2 m, because most points on the ice surface are formed by the intersection of two crevasses. If all four crevasse walls ablate equally, no shift in position will result. This, most horizontal displacement determinations are considered accurate to about 4 m. The down-glacier component of velocity of the lowest 14 km ranges between 2 and 5 m/day, averaged over periods of 27 to 128 days, so the error in velocity may be as large as 7 percent, but the mean error near the centerline is only about 2 percent.

A detailed analysis of the surface-altitude data for flights 9–30 over the lower reach and the lower part of the central basin (Rasmussen and Meier, 1984) indicated that the altitude error in the individual points determined photogrammetrically is about 3.5 m. The recently developed method of optimum interpolation (Gandin, 1963) was used to interpolate altitudes on the same grid on which velocities are given in Fountain (1982). The root-mean-square error in the interpolated values is estimated to be about 2.5 m. The asymmetry of the distribution of the discrepancies between interpolated topography and a sample of 58 points surveyed from the ground suggests that there may be a systematic error of about +1.5 m in the photogrammetrically derived altitude data.

Photogrammetric methods cannot be used to determine the vertical component of velocity directly, because it is the sum of that velocity component and the unknown vertical component of the mass balance rate that is measured; measurement of either component requires markers fixed in the ice.

The horizontal position of the terminus is measured at about 60 points; each point has an error of about 5 m due to both photogrammetric and glaciological error sources. The width-averaged terminus position at any particular time involves the sum of many individual measurements and, therefore, is known more accurately. The accuracy of terminus position averaged over the width, however, is limited by the graphical procedures required to resolve the position of the terminus in the direction of iceflow; this is estimated to be about 5 m.

DATA ACQUIRED

Vertical aerial photographs were obtained for all or part of Columbia Glacier on 44 occasions from July 27, 1974, to January 20, 1984. One earlier flight (July 29, 1957) produced photographs of sufficiently high quality to be used in the analysis. Digital photogrammetry was performed on photographs from 30 flights through September 1, 1981, yielding a total of 6,634 measured points from which surface-altitude and velocity data could be extracted. Additional photogrammetric data were obtained on the configuration of the terminus.

Coordinates were determined for points along the terminus and trackable points widely distributed on the glacier surface. Terminus points were selected in sufficient density to describe the shape of the terminus for each date of aerial photographs. Difficulty was encountered occasionally because of shadows and highly fractured iceblocks.

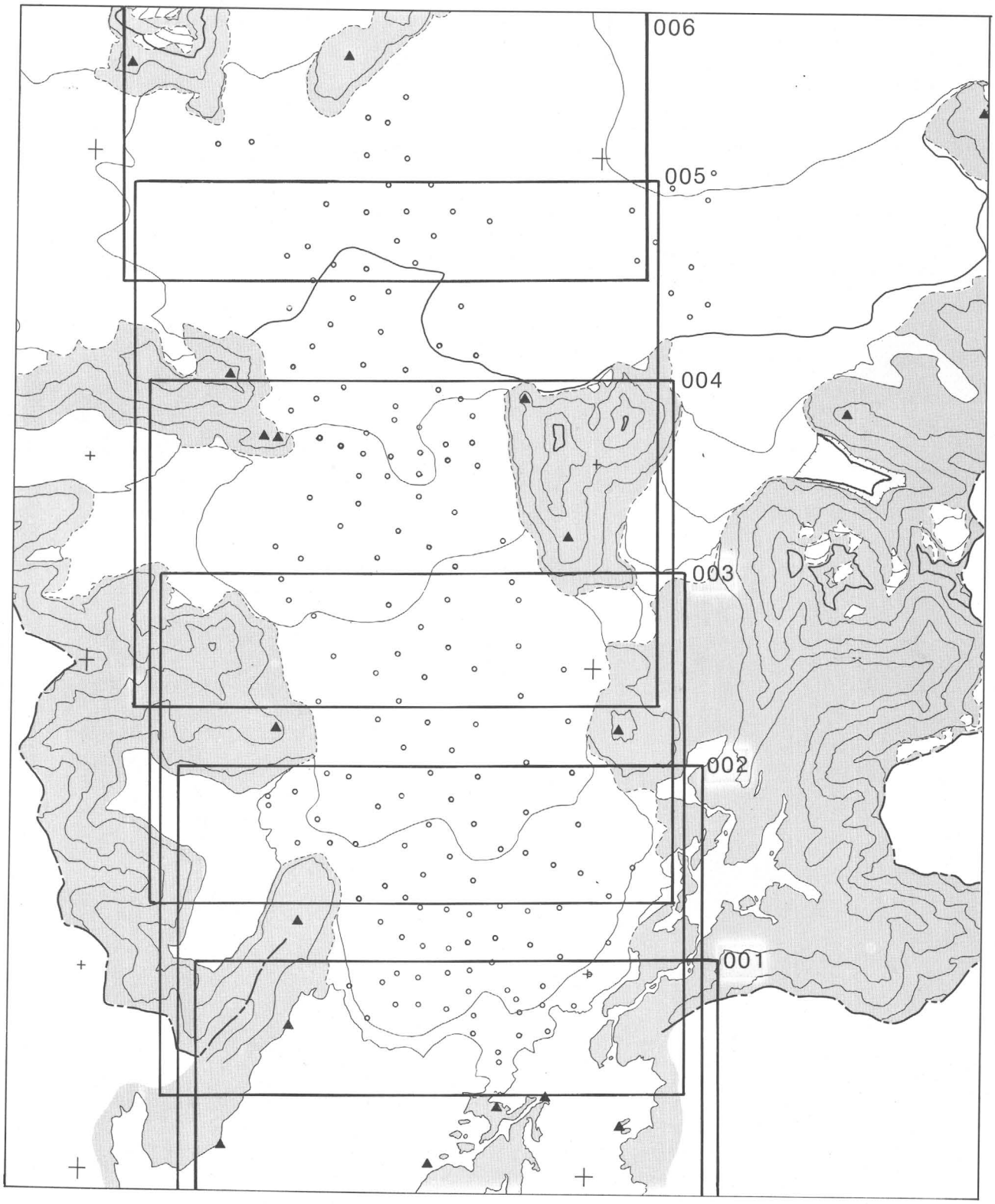

FIGURE 5.—Typical flight plan, showing coverage of each of six vertical aerial photographs. Open circles indicate a typical array of photogrammetrically determined glacier points. Triangles indicate survey stations, used for field control. Contour interval is 100 m.

Ideal locations for glacier points were specified by superimposing a grid over a map of the glacier. For the lower reach of the glacier, 10 columns were arranged parallel to the direction of flow and about 20 rows were arranged perpendicular to the columns. The rows are more closely spaced near the terminus, where the greatest amount of movement occurs. Points were selected as close to the grid intersections as possible, on features that could be tracked from one aerial photographic survey to the next, such as patterns of ice fractures or distinctively shaped iceblocks. A typical distribution of glacier points is shown in figure 5. Point locations were transferred to subsequent photographs by using a precision point-transfer device while simultaneously viewing the photographs for the two dates. The transfer process was one of the critical functions because it directly affected the accuracy of movement measurement. Difficulty was encountered often for areas that produced monotone (uncrevassed) imagery or imagery affected by seasonal factors such as shadows and discoloration, and for areas where the shape of the surface fractures had changed a great deal over time. If the transfer was questionable, the point was eliminated. Over time, points were removed from the glacier by calving and new points were added. The regular pattern of rows and columns became significantly deformed by differential velocity across a row.

To analyze the variations in altitude and velocity along the length of the glacier, a longitudinal coordinate system is defined as shown in figure 6. The origin $\xi=0$ is at the head of the main trunk glacier, and the positive ξ-axis approximately follows the flow centerline to the terminus, which was at $\xi=66.6$ km in 1977–78. It is horizontal and piecewise linear with nodes at 2.0-kilometer in spacing. The transverse coordinate axis has its origin $\zeta=0$ where it crosses the ξ-axis, is normal to the ξ-axis, and is positive to the left as viewed downglacier. Additional longitudinal axes are defined on the major tributaries (fig. 6); their numbering systems are preceded by a letter, and their numerical values correspond to that of the trunk glacier axis where they join it. Informal names have been assigned to various reaches and tributaries to facilitate discussion.

Time t is defined in terms of decimal years, with $t\equiv1978.000$ at 0000 hours on January 1, 1978. Thus,

$$t=1977.99863+0.002737909D \quad (1)$$

where $D=1$ at local noon civil time on January 1, 1978, and increases by 1 for each day thereafter, and the length of the solar year is taken as 365.2422 days (Flammarion, 1880).

Table 1 lists the times, flight altitudes, coverage, and numbers of digitized points for each aerial photographic survey flight.

PHOTOGRAPH OVERLAY

If two vertical aerial photographs of a glacier, taken from nearly the same position at different times and enlarged to the same scale, are overlayed one on the other and then displaced slightly, it may be seen that, in a local area, the crevasse pattern matches from one to the other (fig. 7). Away from this matching area, the crevasses are not juxtaposed, and appear out of focus. However a slight increase or decrease of the displacement moves the sharp (matching) area to another part of the scene. A continuous, slow movement of one photograph relative to the other causes the sharp zone to sweep across the image, tracing out contours of equal displacement at the photograph scale. The displacement at the photograph scale then can be used to calculate the actual displacement and, thus, the velocity of the crevasse pattern in that area.

Several requirements must be met to use the photograph-overlay method: surface features must be distinct and must persist over the time inteval, the part of the glacier of interest must be nearly horizontal, identifiable features of the glacier margins must show in both photographs, and the two photographs must be taken from nearly the same position. Photographs from each date are enlarged to a scale of about 1:10,000 or about 1:20,000. The absolute scale is not nearly as important as the relative scale between sets of photographs, so the scales must be matched as precisely as possible. The sequentially dated, scaled photographs on scale-stable plastic film are overlayed on a light table. With some patience, matching features on the glacier surface, usually crevasses, can be found in local areas on each photograph. After precise alinement, a pinprick is made through the identical features on the (two or three) layered photographs. The photographs then are alined by using fixed features on each side of the glacier as close to the local area as possible. Next, a clean layer of plastic is registered to the fixed features and the pinpricks indicating moving features are transferred to the clean plastic for each sequential photograph. The displacement vector for the time interval is then measured. The local areas, not more than 2–3 km in length, are registered and scaled independently to reduce the magnitude of several possible geometrical errors. Absolute scale of the photographs in the local area is determined by using geographical features along the glacier margins identifiable on both the photographs and a map. The displacement vector then is brought to an absolute value by using the local scale factor.

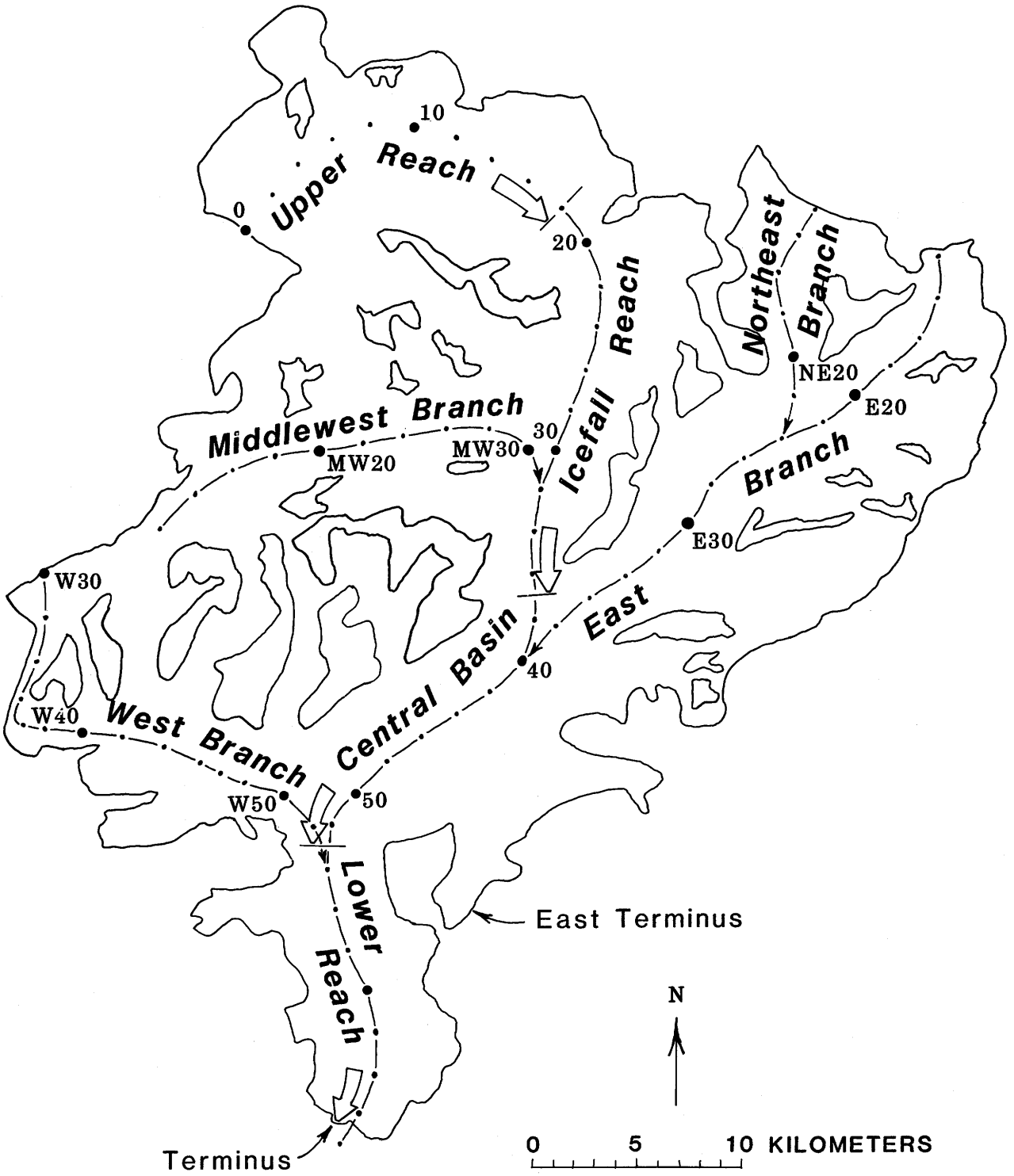

FIGURE 6.—Columbia Glacier, showing longitudinal (ξ) coordinates and informal names of several reaches and tributaries.

TABLE 1.—*Data and coverage of aerial photography*

[Coverages are designated as follows: a, most of glacier; b, whole glacier; c, lowest 4 km; d, lower reach; e, icefall reach; and f, central basin]

Flight No.	Date	*t*	Flight altitude (m)	Coverage	Number of digitized locations				
					Terminus	Lower reach	Icefall reach	Other	Total
	1957								
1.	July 29	1957.574	9,000	a	36	214	10	42	302
	1974								
2.	July 27	1974.568	7,920	b	15	210	. . . . .	. . . . .	566
	1976								
3.	July 24	1976.561	5,490	c	17	137	. . . . .	. . . . .	154
4.	Oct. 1	.750	5,490	c	14	148	. . . . .	. . . . .	162
5.	Nov. 17	.879	5,490	c	20	73	. . . . .	. . . . .	93
	1977								
6.	Jan. 19	1977.051	5,490	c	22	68	. . . . .	. . . . .	90
7.	Mar. 7	.180	5,490	c	24	64	. . . . .	. . . . .	88
8.	Apr. 23	.309	5,490	c	27	154	. . . . .	. . . . .	181
9.	June 2	.418	5,490	d	22	172	. . . . .	24	28
10.	July 7	.514	7,010	d	19	184	. . . . .	38	241
11.	Aug. 29	.659	7,010	d	28	185	. . . . .	42	255
12.	Nov. 8	.854	7,010, 8,230	d, f	23	169	. . . . .	33	225
	1978								
13.	Feb. 28	1978.160	6,400	d	26	171	. . . . .	31	228
14.	Apr. 19	.297	7,010, 7,770	d, e, f	34	167	. . . . .	26	227
15.	June 11	.442	7,010, 7,770	d, e, f	29	159	53	60	301
16.	July 30	.576	7,010, 8,530	d, e, f	39	158	53	36	282
17.	Aug. 26	.650	7,010	d	81	168	. . . . .	25	274
18.	Nov. 8	.853	5,490	d	76	164	. . . . .	29	269
	1979								
19.	Jan. 6	1979.014	6,100	d	63	140	. . . . .	29	232
20.	Apr. 12	.277	7,010	d	70	146	. . . . .	29	245
21.	Aug. 18	.628	7,010	d	54	129	. . . . .	22	205
22.	Oct. 20	.800	7,010	d	58	138	. . . . .	24	220
	1980								
23.	Feb. 29	1980.162	7,010	d	78	128	. . . . .	18	224
24.	May 12	.361	7,010	d	86	128	. . . . .	21	235
25.	July 22	.556	7,010	d	77	117	. . . . .	17	211
26.	Sept. 2	.671	7,010	d	92	116	. . . . .	14	222
27.	Oct. 30	.830	7,010	d	98	113	. . . . .	14	225
	1981								
28.	Mar. 7	1981.180	7,010	d	94	112	. . . . .	13	219
29.	June 16	.457	7,010	d	92	110	. . . . .	13	215
30.	Sept. 1	.667	7,010	d	92	110	. . . . .	13	215
31.	Sept. 26	.736	6,400	d	. . . . .	. . . . .	. . . . .	. . . . .	. . . . .
32.	Nov. 15	.873	7,010	d	. . . . .	. . . . .	. . . . .	. . . . .	. . . . .
	1982								
33.	Jan. 22	1982.059	7,010	d	. . . . .	. . . . .	. . . . .	. . . . .	. . . . .
34.	Mar. 31	.245	7,010	d	. . . . .	. . . . .	. . . . .	. . . . .	. . . . .
35.	Aug. 2	.585	7,010	d	. . . . .	. . . . .	. . . . .	. . . . .	. . . . .
36.	Oct. 15	.787	7,010	d	. . . . .	. . . . .	. . . . .	. . . . .	. . . . .
	1983								
37.	Jan. 21	1983.056	7,010	d	. . . . .	. . . . .	. . . . .	. . . . .	. . . . .
38.	Mar. 7	.179	7,010	d	. . . . .	. . . . .	. . . . .	. . . . .	. . . . .
39.	Apr. 7	.264	7,010	d	. . . . .	. . . . .	. . . . .	. . . . .	. . . . .
40.	June 17	.458	7,010	d	. . . . .	. . . . .	. . . . .	. . . . .	. . . . .
41.	Aug. 19	.631	7,010	d	. . . . .	. . . . .	. . . . .	. . . . .	. . . . .
42.	Sept. 16	.707	7,010	d	. . . . .	. . . . .	. . . . .	. . . . .	. . . . .
43.	Nov. 6	.847	7,010	d	. . . . .	. . . . .	. . . . .	. . . . .	. . . . .
44.	Dec. 8	.934	7,010	d	. . . . .	. . . . .	. . . . .	. . . . .	. . . . .
	1984								
45.	Jan. 20	1984.052	7,010	d	. . . . .	. . . . .	. . . . .	. . . . .	. . . . .

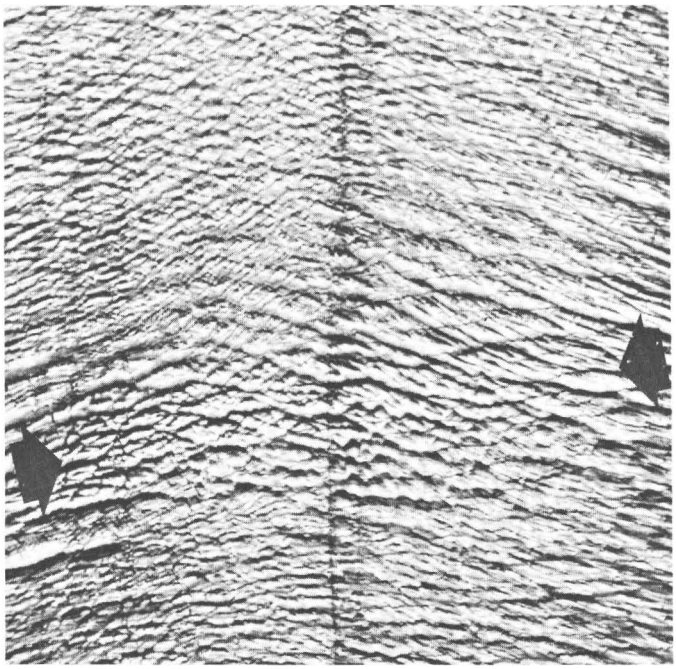

FIGURE 7.—Superimposed portions of vertical aerial photographs illustrating the photograph-overlay method. The two photographs, taken on September 26 and November 15, 1981, are displaced about 190 m in the north-south direction. Note that in an area between the two arrows the image appears sharp, whereas above and below that, the image area appears doubled and confused. The sharp area marks a zone of constant displacement (velocity). North is to the top, and flow is from top to bottom. This area of the glacier is about 950 m wide and is located near the center of the glacier at $\xi \approx 64.4$ km. The vertical dark band is a streak of debris on the ice (medial moraine).

The direct photograph-overlay procedure is less costly and is quicker than photogrammetric methods, but it is appreciably less accurate. The overlay procedure generally can be used to locate points to within 20 to 50 m and costs roughly $1 per point, compared with a photogrammetric location error of about 2 m and a cost of about $20 per point. This simple photograph-overlay method was used to fill in gaps on the velocity map of Columbia Glacier in some areas of rapid movement and to measure the velocity of other calving glaciers, such as Hubbard Glacier, where data were needed to determine calving speed (Brown and others, 1982).

The largest source of error when using the photograph-overlay method is in correcting for the displacements of points from their planimetric positions that are caused by relief between the exposure point (the projection of the principal point or center point of the aerial photograph onto the ground) and the glacier points to be measured. Points that on the ground are at higher altitudes than the exposure points are displaced radially outward toward the edges of the photograph; points at lower altitudes than the exposure point are displaced inward. Most of the data obtained by direct-overlay methods were not corrected for relief displacement, but limited use was made of graphical radial-line triangulation or simple analytical techniques. Errors attributable to other sources—Earth curvature, atmospheric refraction, and radial lens distortion—are probably less than ± 1 mm on the aerial photograph at the 1:20,000 working scale used in this study and are, therefore, ignored. Errors caused by tilting of photographs intended to be vertical may be significant.

OGIVE SPACING

An appreciable area of the upper part of Columbia Glacier is a complex filigree of snow fingers, small icefalls, and compound tributaries where ice and snow move off high ridges to join the larger ice streams below. It is difficult to obtain velocity data in this area, but some scattered values could be obtained by the measurement of ogive spacing.

Wave ogives (fig. 8) form annually at the base of many icefalls, owing to the seasonal variation of accumulation or ablation on ice that is seasonally stretched as it rides through the icefall (Nye, 1959; Waddington, 1981). If the iceflow is steady, the spacing of ogives at one location is a measure of annual surface velocity at that location. If the flow is not steady, ogive spacing departs from the current annual velocity and the departure increases with the age of the ogive and the change in the velocity field over time.

The extensive aerial photography of Columbia Glacier reveals 19 sets of wave ogives that could be measured to estimate annual velocity. Only the most recent pair in each set is measured to minimize the effects of nonsteady flow. Numerous dirt-band ogives, which persist long after wave ogives have disappeared, occur on Columbia Glacier notably along most of the length of the East Branch. Measurements of these dirt-band ogives show major discrepancies with current velocity, in the sense that the velocity field has decreased markedly over time. Therefore, no dirt-band ogives are used in this study.

The accuracy of determining annual velocities from ogive measurements is limited by the difficulty of defining ogive crests or troughs and by the error involved in reconstructing true scale from aerial photographs in these areas of high relief. The error in annual velocity is estimated at 10 percent for velocities ranging from 10 to 300 m/a.

STAKE MEASUREMENTS

Metal stakes were set in the snow or ice surface at about 60 locations and were surveyed at the beginning

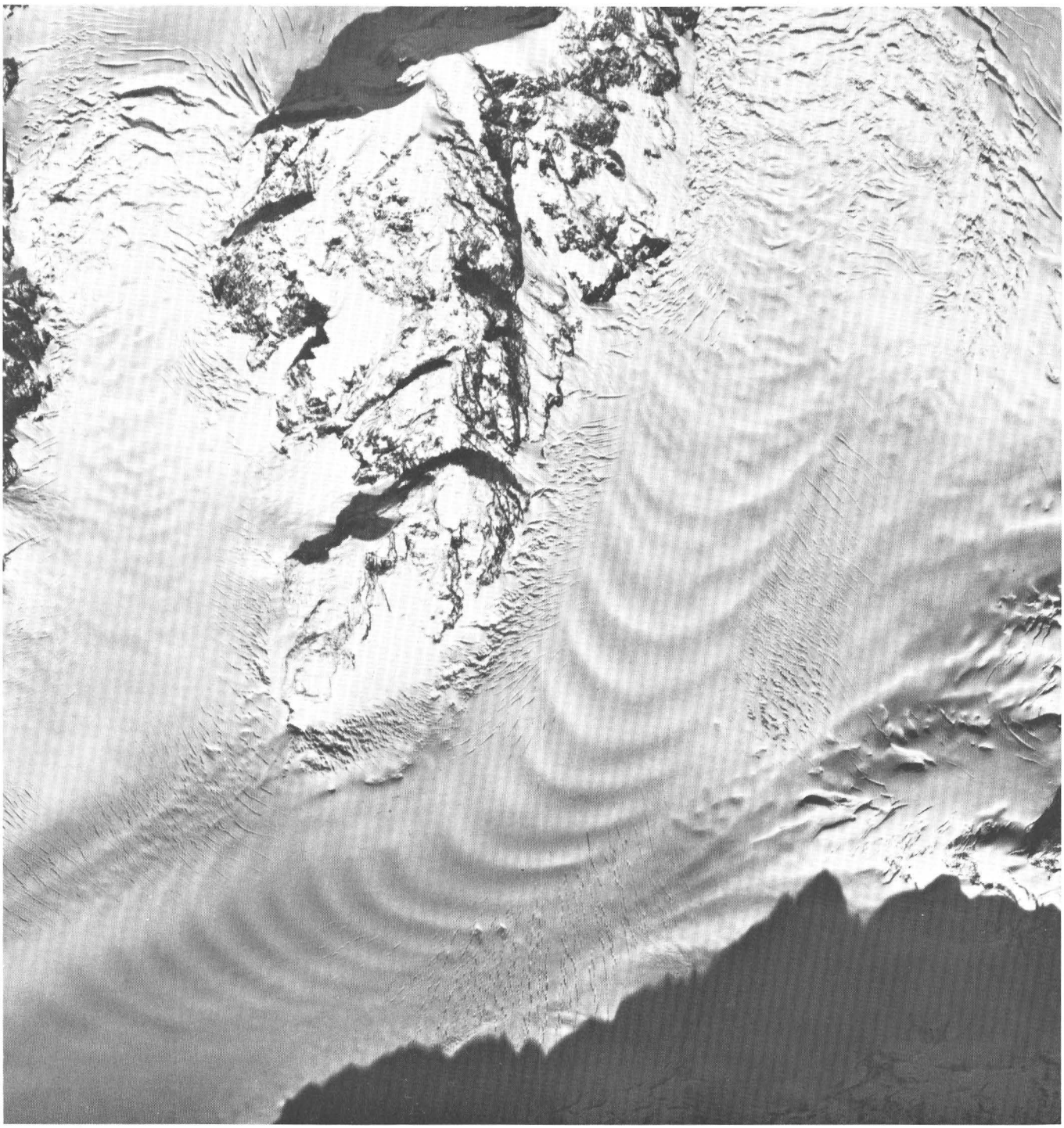

FIGURE 8.—Vertical aerial photograph from about 7,000 m above sea level showing wave ogives downglacier from an unnamed icefall upglacier from the west branch of Columbia Glacier, September 26, 1981.

and at the end of the 1977–78 measurement year (Mayo and others, 1979). The altitude of the glacier surface was measured at each stake and at three points forming a triangle around each stake. The error in horizontal position is about 0.1 m. The error in ice-surface altitude ranges between 0.05 and 1.0 m, depending on the distance from survey stations and the roughness of the ice surface. Coordinate information as well as the methodology and estimation of errors were given in Mayo and others (1979).

SURFACE ALTITUDE

Surface topographic maps of the lower reach and the lower part of the central basin were prepared at a 10-meter contour interval for flight 2 by the U.S. Geological Survey, Western Mapping Center at Menlo Park, Calif., and for flight 30 by Air Photo Tech of Anchorage, Alaska. For flights 1 to 30, altitudes were determined photogrammetrically by the Western Mapping Center.

Because data on the nodes of a square grid are the ideal form for use with numerical models, altitudes were interpolated on 154 nodes of the 0.7625-kilometer grid (Fountain, 1982; Rasmussen and Meier, 1984). This was done for the 22 flights 9 through 30. The method of optimum interpolation (Gandin, 1963), which is widely used in meteorology, was used. This method tends toward using all the data, provides an independent estimate of the interpolation error, and, to the degree that the statistical structure of the interpolated variable is known, minimizes that error. The statistical structure of the surface topography is described in terms of the correlation between the altitude changes at some point and the changes at some other point. In this region of Columbia Glacier, this correlation has a high degree of homogeneity and isotropy, both spatially and temporally, and is not affected much by the glacier flow. This remarkable regularity permits using a very simple implementation of the optimum interpolation algorithm.

The best fitting linear combination of the two maps is used as the first approximation of the topography for the date of any one of the 22 flights. The deviations of the irregularly positioned points about the linear combination are the variables actually interpolated. Because the time rate of change of the surface altitude has profound glacier-dynamics implications, as expressed by the equation of continuity, the interpolation is conducted in the three-dimensional x,y,t domain. To interpolate the altitude of a particular node for a particular flight, irregularly positioned points up to 1 km distant and separated in time by up to 0.39 a were used.

The surface topography of the lower reach of the glacier on 1957.574, 1974.568, 1977.659, and 1981.667 are presented as plates 1*A–D*. The 1974 map was drawn by photogrammetry, the 1981 map was derived by smoothing a photogrammetric map, and the 1977 map was derived from photogrammetric point values interpolated to a rectangular grid by the method of optimum interpolation and contoured by hand. It is apparent that the lower reach of the glacier has thinned increasingly rapidly from 1957 to 1974, from 1974 to 1977, and from 1977 to 1981.

The change in surface altitude during the approximate measurement year 1977.659 to 1978.650 is shown on plate 2. The change was derived by subtracting gridded, interpolated values for these two times and hand-contouring the result. A field obtained by using the CalComp General Purpose Contouring Program by California Computer Products, Inc., showed a great amount of apparent noise, ranging from more than +12 m to less than −21 m of change for the same period. Plate 2 shows changes ranging from +2 to −12 m and is a relatively smooth field. Thus, careful attention to the structure of the field in space and time, by use of a method such as optimum interpolation, is necessary. Thinning during the measurement year increased from just under 5 m at the upper end of the lower reach to between 5 and 10 m in the reach $58 < \xi < 66$ km (exceeding 10 m at only four grid points) but decreasing to about 0 at the terminus.

TERMINUS CONFIGURATION

MAPPING OF THE TERMINUS

As part of the digital photogrammetric processing of vertical aerial photographs, points were determined at the intersection of the sea surface and the calving terminus west of Heather Island (fig. 1). In the last few weeks of 1978, the ice front broke away from Heaher Island, extending the ice front farther east, and photogrammetric determinations of the position of the terminus were extended to the east. The configuration of the terminus was mapped by using the photogrammetric locations for control and by using a vertical aerial photograph carefully enlarged to a scale of 1:20,000 or 1:10,000 to fill in detail and (prior to 1979) to extend the mapping farther east. Mapping since 1981.667, except for 1982.245, was done without photogrammetric control.

The accuracy of determining the coordinates of a single point using photogrammetry is about 3 m, and the accuracy of determining single points along a boundary mapped without photogrammetric control is estimated at between 10 and 20 m, depending mainly on the tile of the aerial camera.

The altitude of the ice surface at the terminus (ice-cliff height) is not yet well known. The approximate ice-surface configuration was determined by photogrammetric mapping for the 1974.568 (pl. 1*B*) and 1981.667 (pl. 1*D* and pl. 3) flights, although it is not known how the photogrammetrist followed the mean configuration of the ice surface over such an irregular, broken area (figs. 3, 9).

The 1981.667 topography of the land and the ice surface near the terminus is shown in plate 3. In addition, the seabed topography is shown where it could be mapped by Austin Post (written commun., 1982) using bathymetric sounding from the research vessel *Growler* and

FIGURE 9.—Oblique aerial photograph of a part of the terminus, showing rough surface near the terminus ice cliff, October 8, 1975. U. S. Geological Survey photograph No. 75M5–54, by L. R. Mayo.

the radio-controlled skiff *Bergy Bit*. The fields overlap because bathymetric measurements could be made in 1978–80 and in 1982–83 in areas occupied by ice in 1981.

The 1981.667 ice cliff ranged in height from less than 50 m to more than 80 m. The calving ice face was in water from 0 to more than 200 m (perhaps 220 m) deep, so the ice face ranged in thickness from less than 50 to about 300 m. Also shown in plate 3 is a major shoal between Heather Island and the mainland to the west. This shoal rises more than 200 m from a gently sloping seabed to less than 30 m below mean lower low water (zero of the conventional tidal datum). Radar soundings indicate that the channel a few kilometers upglacier from the shoal is as much as 400 m below sea level (Vickers and Bollen, 1974; Rasmussen and Meier, 1982).

Calving is high in summer (Sikonia and Post, 1980), causing a retreat from midsummer into fall. This is illustrated by plate 4*A*, which shows changes between the seven flights spanning the 1977–78 measurement year. Clearly shown is a large embayment that continued to enlarge in the fall, closed in winter and spring, and reached an embayment minimum (most extended position) at the beginning of summer. This was followed by the formation of a new embayment.

Vertical aerial photographs were available within 3 weeks of August 1 for the years 1957, 1974, and 1976–83. Maps of the terminus at these times are shown on plate 4*B*. These results, and those for additional years reported by Post (1975) and Sikonia and Post (1980), show that recession was relatively slight until it intensified in 1978. Perhaps more emphatically revealing the recession, maps of the terminus at the time in fall of the annual minimum (pl. 4*C*) show the remarkable, continuous retreat of the eastern two-thirds of the terminus from 1976 through 1983.

TABLE 2.—*Width-averaged position of the terminus <Ξ> through time*

[Methods are designated as follows: a, digital photogrammetry; b, photograph overlay; c, field surveys using angles to water surface from distant high point; d, field surveys using angles to water surface from Heather Island; e, shipborne radar]

Flight No.	Date	t	<Ξ>	Method
	1957			
1.	July 29	1957.574	66.84	a
	1974			
2.	July 27	1974.568	66.79	a
	1976			
3.	July 24	1976.561	66.75	a
4.	Oct. 1	.750	66.56	a
5.	Nov. 17	.879	66.55	a
	1977			
6.	Jan. 19	1977.051	66.63	a
7.	Mar. 7	.180	66.65	a
8.	Apr. 23	.309	66.73	a
9.	June 2	.418	66.78	a
10.	July 7	.514	66.76	a
11.	Aug. 29	.659	66.51	a
12.	Nov. 8	.854	66.46	a
	1978			
13.	Feb. 28	1978.160	66.59	a
14.	Apr. 19	.297	66.64	a
15.	June 11	.442	66.70	a
16.	July 30	.576	66.62	a
17.	Aug. 26	.650	66.54	a
18.	Nov. 8	.853	66.37	a
	1979			
19.	Jan. 6	1979.014	66.44	a
20.	Apr. 12	.277	66.61	a
21.	Aug. 18	.628	66.55	a
22.	Oct. 20	.800	66.36	a
	1980			
23.	Feb. 29	1980.162	66.47	a
24.	May 12	.361	66.61	a
25.	July 22	.556	66.61	a
26.	Sept. 2	.671	66.59	a
27.	Oct. 30	.830	66.50	a
	1981			
28.	Mar. 7	1981.180	66.60	a
	June 7	.432	66.64	c
29.	June 16	.457	66.64	a
	Aug. 5	.594	66.51	c
	1981—Continued			
30.	Sept. 1	1981.667	66.34	a
31.	Sept. 26	.736	66.28	e
	Oct. 25	.815	66.17	e
32.	Nov. 15	.873	66.15	b
	1982			
	Jan. 12	1982.048	66.23	c
33.	Jan. 22	.059	66.20	b
34.	Mar. 31	.245	66.32	a
	June 11	.442	66.45	c
35.	Aug. 2	.585	66.33	b
	Aug. 9	.604	66.32	d
	Aug. 10	.607	66.30	d
	Aug. 11	.609	66.29	d
	Aug. 12	.612	66.30	d
	Aug. 16	.650	66.25	c
	Sept. 3	.672	66.22	e
	Sept. 25	.732	66.11	e
	Sept. 30	.746	66.08	e
36.	Oct. 15	.787	66.05	b
	Oct. 30	.828	66.00	e
	1983			
	Jan. 5	1983.012	66.05	b
	Jan. 8	.020	66.04	c
37.	Jan. 21	.056	66.06	b
38.	Mar. 7	.179	66.16	b
39.	Apr. 7	.264	66.20	b
40.	June 17	.458	66.28	b
41.	Aug. 19	.631	66.10	b
42.	Sept. 16	.707	65.94	b
	Sept. 21	.721	65.91	e
	Sept. 27	.737	65.85	e
	Sept. 29	.743	65.83	e
	Oct. 11	.776	65.82	e
	Oct. 25	.814	65.77	e
43.	Nov. 6	.847	65.75	b
	Nov. 12	.863	65.70	e
44.	Dec. 8	.934	65.67	b
	1984			
	Jan. 15	1984.038	65.57	c
45.	Jan. 20	.052	65.59	b

VARIATIONS OF GLACIER LENGTH

A single value of glacier length measured along any particular flowline fixed in space would not be representative of the entire glacier because embayments change the terminus shape markedly over time. A value averaged over the active portion of the glacier is better. An average value is determined by reading individual length values off the (ξ,ζ) net in the vicinity of the terminus, with ξ-trajectories parallel to the mean trajectories of iceflow during the measurement year, ζ-trajectories normal to those of ξ, and with a 250-meter grid spacing at (66.0,0) (pl. 4*A*). The individual length values, designated Ξ, are read at 15 or more points where the terminus intersects the ξ-trajectories over $-2.0<\zeta<1.5$ km. The average produces a mean value for glacier length $\langle\Xi\rangle$.

The error in an individual Ξ when controlled by photogrammetry is estimated to be 10 m, and when not controlled by photogrammetry, 14 to 22 m. Thus, the accuracy of $\langle\Xi\rangle$ might be from 3 to 6 m, except that some fixed errors of a similar amount may occur in the overlaying and reading processes. Therefore, the final numerical results are considered correct to 10 m or so.

Table 2 presents values of $\langle\Xi\rangle$ for each aerial photographic survey flight. In addition, values obtained by techniques other than digital photogrammetry and photograph overlay are listed. These include measurements of vertical and horizontal angles to the water surface by theodolite from a high, distant survey station (L. R. Mayo, written commun., 1982) and from a low point on Heather Island (R. M. Krimmel, written commun., 1982), and measurement from radar onboard the research vessel *Growler* (Austin Post, written commun., 1982–83). The other methods are less accurate than photogrammetry. The individual values of $\Xi(\zeta,t)$ are given in table 3.

Using the data of table 3, a plot of glacier length Ξ against transverse distance ζ and time (fig. 10) shows how the terminus configuration has been changing. A "ridge" of extended length at $\zeta \sim 1.25$ km existed until late 1978; this was a part of the glacier that terminated on Heather Island and, therefore, was protected from calving. The ice peninsula connecting the glacier to the island was breached in late December 1978, increasing the width of the terminus that was exposed to calving.

Prominent embayments (minimums in glacier length) occurred in late 1976, 1977, 1978, and 1979. Each year the embayments were deeper and a little farther east. Then, in late 1980, the pattern changed, and beginning in late 1981 recession broadened and deepened both east and west, with only a narrow zone at $\zeta \sim -1.2$ km continuing, until late 1983, to resist recession.

The $\langle\Xi\rangle$ data presented in table 2 reveal a slight but accelerating long-term retreat on which is superimposed a large seasonal fluctuation (fig. 11). This effect is displayed most clearly by folding each year into a single January to December scale (fig. 12). The strong seasonal fluctuation is seen to be consistent from year to year, except for the second half of 1980. The maximum occurs at 0.46 ± 0.02 a (June 17 ± 7 days), and the minimum of 0.87 ± 0.05 a (November 13 ± 20 days). The seasonal amplitude is 370 ± 130 m. The average rate of recession from 1977 to 1980 was only 22 m/a, but for 1981–82 it accelerated to 180 m/a, and in 1982–83 it further accelerated to 360 m/a.

The behavior of the glacier in the second half of 1980 clearly was unusual; the seasonal retreat was only 160 m, whereas the average seasonal retreat for other years was 409 m. Apparently, the calving rate was extremely low that year.

VELOCITY AND STRAIN-RATE MEASUREMENTS

SPATIAL DISTRIBUTION OF VELOCITY OVER THE ENTIRE GLACIER

The inferred distribution of the horizontal component of surface velocity during the measurement year for the entire Columbia Glacier is shown on plate 5. A total of 1,796 photogrammetry measurements, 207 photograph-overlay measurements, 56 stake-motion measurements, and 12 ogive-spacing measurements was used for inferring this velocity distribution, with the highest measurement density in the lower reach and the icefall reach. Figure 13 shows velocity along the centerline as a function of longitudinal distance for the main glacier and its tributaries.

The pattern of speed shows that the main glacier flows much more rapidly than any of its tributaries and attains very high speeds (exceeding 1 km/a) in the icefall reach and in the lower reach. This pattern is reminiscent of an ice stream in an ice sheet. A more complete discussion of the velocity and strain-rate fields in the icefall reach and the lower reach follows.

VELOCITY AND STRAIN RATE IN THE ICEFALL REACH

Iceflow in this reach had to be measured as accurately as possible so that when the measurements were combined with thickness data, the discharge from the accumulation area to the ablation area of the main stem of Columbia Glacier could be estimated. Estimation was required because only nine stakes were placed in the accumulation area to measure annual balance and thickness change; this was an inadequate sampling density for this huge area of complex geometry and varied altitude. The photograph-overlay method was used to supplement data from photogrammetric measurements and three stake surveys. Vertical aerial photographs were acquired on April 19, June 11, and July 30, 1978. Position data for points along the approximate flow centerline are given in table 4.

The velocity in this reach shows great spatial variation, especially above $\xi = 28$ km. Thus, stakes or points may move from areas of high velocity to areas of low velocity, or vice versa. The true spatial variation of the velocity must then be inferred from the endpoints of the trajectories of the stakes and the photogrammetric points.

The centerline velocity distribution for the upper icefall reach ($17 < \xi < 28$ km) is inferred from the initial (t_0,ξ_0) and final (t_1,ξ_1) positions on the trajectories of 41 identifiable surface features observed by photograph-overlay methods from vertical aerial photographs acquired on April 19 and July 30, 1978. The velocity distribution $v_\xi = g(\xi)$ is defined to be the one that, had it

TABLE 3.—*Terminus position Ξ, in kilometers, as a function of transverse distance ζ and flight number (see table 1)*

[Note: 60.00 kilometers should be added to each Ξ value]

Flight No.	Transverse distance, ζ, in km														
	−2.00	−1.75	−1.50	−1.25	−1.00	−0.75	−0.50	−0.25	0.00	0.25	0.50	0.75	1.00	1.25	1.50
1.	6.51	6.61	6.66	6.86	6.86	6.91	7.06	7.01	6.96	6.96	6.96	6.91	7.06	7.11	6.18
2.	5.86	5.96	6.51	6.61	6.81	6.96	7.01	7.11	7.11	6.96	7.06	7.21	7.16	7.16	6.31
3.	6.07	6.33	6.55	6.81	6.87	6.96	6.80	6.61	6.61	6.87	7.02	7.05	7.21	7.16	6.26
4.	6.03	6.25	6.60	6.79	6.86	6.62	6.41	6.23	6.19	6.24	6.51	6.98	7.16	7.11	6.36
5.	6.15	6.20	6.56	6.71	6.85	6.62	6.45	6.31	6.23	6.31	6.53	6.81	7.11	7.11	6.36
6.	6.27	6.36	6.57	6.71	6.87	6.67	6.57	6.47	6.47	6.51	6.66	6.81	7.02	7.16	6.36
7.	6.20	6.21	6.53	6.73	6.93	6.73	6.73	6.62	6.53	6.59	6.71	6.83	6.93	7.16	6.36
8.	6.25	6.25	6.57	6.86	6.93	6.87	6.81	6.80	6.71	6.71	6.81	6.85	6.95	7.16	6.41
9.	6.31	6.31	6.61	6.87	6.91	6.93	6.91	6.90	6.81	6.81	6.91	6.91	6.95	7.11	6.41
10.	6.29	6.31	6.63	6.85	6.86	6.97	6.92	6.91	6.77	6.69	6.85	6.89	6.93	7.16	6.41
11.	6.35	6.26	6.56	6.79	6.85	6.89	6.79	6.26	6.11	5.83	6.09	6.39	6.89	7.16	6.46
12.	6.29	6.26	6.51	6.71	6.73	6.61	6.28	6.15	6.11	6.15	6.22	6.56	6.83	7.21	6.31
13.	6.27	6.26	6.56	6.73	6.76	6.60	6.51	6.51	6.51	6.55	6.59	6.71	6.83	7.16	6.36
14.	6.21	6.26	6.56	6.69	6.76	6.69	6.63	6.65	6.69	6.69	6.70	6.75	6.86	7.11	6.36
15.	6.21	6.29	6.59	6.66	6.87	6.79	6.79	6.80	6.77	6.75	6.83	6.87	6.85	7.11	6.36
16.	6.35	6.27	6.57	6.67	6.79	6.89	6.79	6.75	6.77	6.30	6.33	6.46	6.84	7.11	6.41
17.	6.34	6.26	6.56	6.66	6.83	6.86	6.79	6.70	6.75	6.27	6.15	6.15	6.31	7.11	6.41
18.	6.26	6.21	6.36	6.65	6.79	6.86	6.81	6.61	6.36	6.19	6.07	5.93	6.01	6.11	6.36
19.	6.29	6.17	6.36	6.69	6.83	6.94	6.93	6.75	6.51	6.36	6.23	6.13	6.11	6.11	6.26
20.	6.27	6.21	6.41	6.76	6.91	6.97	6.98	6.92	6.83	6.78	6.61	6.46	6.37	6.31	6.31
21.	6.16	6.11	6.66	6.89	6.87	6.92	6.61	6.45	6.51	6.61	6.61	6.61	6.49	6.31	6.41
22.	6.13	6.11	6.63	6.83	6.81	6.65	6.61	6.55	6.53	6.13	5.89	5.80	6.03	6.26	6.41
23.	6.06	6.12	6.75	6.87	6.89	6.86	6.72	6.60	6.51	6.45	6.29	6.16	6.17	6.21	6.41
24.	6.09	6.23	6.83	6.94	6.94	6.95	6.93	6.77	6.77	6.65	6.65	6.40	6.31	6.26	6.42
25.	6.09	6.22	6.85	6.90	6.92	6.94	6.86	6.81	6.85	6.80	6.69	6.58	6.22	6.02	6.44
26.	6.06	6.16	6.81	6.89	6.88	6.93	6.84	6.80	6.87	6.78	6.71	6.56	6.22	5.98	6.34
27.	6.00	6.11	6.75	6.86	6.87	6.92	6.79	6.69	6.81	6.69	6.45	6.37	6.18	6.00	5.94
28.	6.00	6.23	6.82	6.95	6.96	7.01	6.88	6.78	6.93	6.93	6.68	6.45	6.30	6.18	5.92
29.	5.98	6.36	6.92	6.94	6.95	6.98	7.00	6.97	7.01	6.91	6.74	6.55	6.21	6.17	5.98
30.	5.96	6.31	6.88	6.88	6.88	6.95	6.83	6.74	6.70	6.61	5.53	5.42	5.55	5.77	6.04
31.	6.00	6.36	6.88	6.89	6.87	6.78	6.64	6.60	6.59	6.58	5.49	5.34	5.47	5.65	6.01
32.	5.89	6.26	6.84	6.82	6.75	6.63	6.44	6.20	6.06	5.99	5.82	5.59	5.54	5.57	5.92
33.	5.88	6.28	6.80	6.78	6.79	6.71	6.57	6.38	6.29	6.12	5.86	5.66	5.63	5.60	5.69
34.	5.91	6.24	6.82	6.78	6.91	6.78	6.63	6.65	6.55	6.47	6.21	5.91	5.71	5.67	5.49
35.	5.92	6.36	6.81	6.89	6.94	6.92	6.76	6.70	6.78	6.78	5.61	5.57	5.67	5.86	5.31
36.	5.87	6.36	6.81	6.92	6.82	6.63	6.17	6.05	6.00	5.86	5.66	5.53	5.42	5.38	5.28
37.	5.79	6.27	6.72	6.93	6.82	6.44	6.28	6.25	6.17	5.63	5.75	5.63	5.51	5.41	5.26
38.	5.83	6.31	6.73	6.95	6.81	6.63	6.53	6.49	6.17	6.10	5.87	5.71	5.61	5.42	5.24
39.	5.83	6.31	6.73	6.95	6.85	6.72	6.59	6.55	6.31	6.18	5.96	5.69	5.60	5.47	5.25
40.	5.89	6.36	6.76	6.96	6.96	6.68	6.71	6.69	6.67	6.57	6.15	5.67	5.47	5.45	5.27
41.	5.67	6.31	6.63	6.95	6.77	6.66	6.43	6.35	6.25	6.13	5.66	5.47	5.43	5.45	5.26
42.	5.67	6.33	6.60	6.95	6.67	6.28	6.05	5.97	5.83	5.71	5.62	5.47	5.42	5.43	5.15
43.	5.55	6.01	6.51	6.75	6.21	6.02	5.89	5.73	5.54	5.44	5.39	5.49	5.53	5.17	5.03
44.	5.53	5.99	6.43	6.27	6.13	6.12	6.01	5.78	5.59	5.45	5.33	5.23	5.17	5.04	5.02
45.	5.47	5.99	6.21	6.22	6.13	6.20	6.01	5.89	5.75	5.53	5.38	5.27	5.21	5.07	5.02

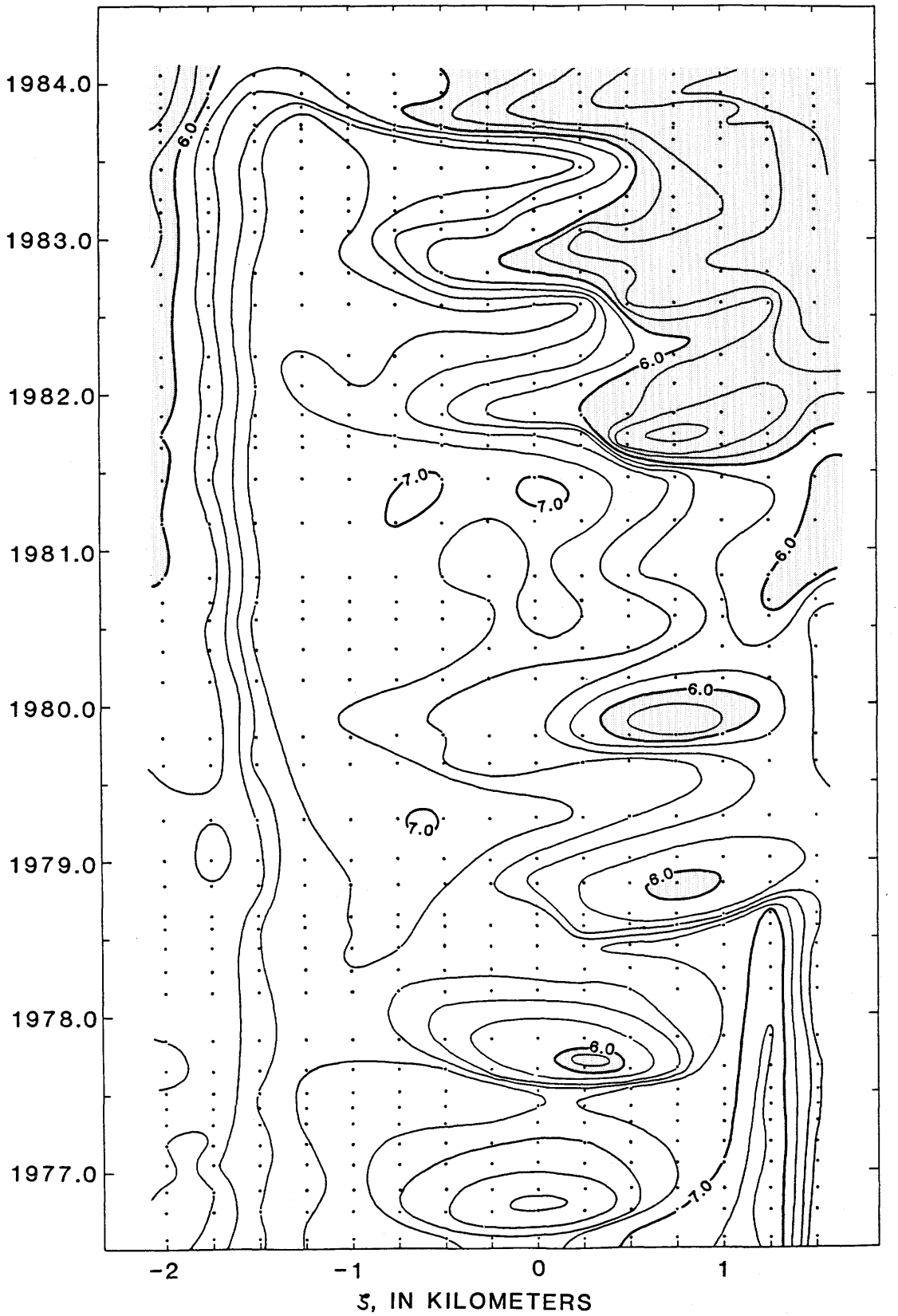

FIGURE 10.—Diagram showing position of the terminus Ξ as a function of transverse distance ξ and time. The contoured variable is the amount (in kilometers) by which the distance from the head of the glacier exceeds 60 km; area with values less than 6.0 (66.0 km) are stippled. The approximate western border of the terminus is along the left margin of the diagram; the eastern border of the terminus is to the right of the right margin.

TABLE 4.—*Velocities V_ξ measured near the centerline in the reach $17<\xi<37$ km*

[Some velocity values are missing because the point could not be identified on one or another of the photographs]

Point No.	t_0	t_1	ξ_0 (km)	ξ_1 (km)	$\bar{\zeta}$ (km)	V_ξ (km/a)
A. Stake measurements						
24	1977.656	1978.647	24.003	24.991	0.007	0.994
28.2	1977.659	1978.650	28.272	28.715	−.210	.450
32	1977.659	1978.650	32.069	33.034	.148	.975
B. Photogrammetric measurements (t_0=1978.442, t_1=1978.576)						
7402	.....	.....	23.909	24.080	0.166	1.014
7302	.....	.....	25.110	25.224	.348	.899
6903	.....	.....	28.474	28.547	.274	.555
6802	.....	.....	29.681	29.783	1.135	.859
6702	.....	.....	30.977	31.115	1.050	1.045
6602	.....	.....	31.627	31.765	.994	1.032
6503	.....	.....	32.057	32.192	−.010	1.006
6402	.....	.....	33.473	33.625	.787	1.155
6302	.....	.....	34.043	34.196	.866	1.163
6203	.....	.....	35.408	35.553	−.065	1.098
6103	.....	.....	36.212	36.351	.376	1.050
6003	.....	.....	37.307	37.420	−.042	.852

$\bar{\xi}$ (km)	$\bar{\zeta}$ (km)	V_ξ (km/a)		
		t_0 to t_1	t_1 to t_2	t_0 to t_2
C. Photograph-overlay measurements (t_0=1978.297, t_1=1978.442, t_2=1978.576)				
17.0	0.1	0.33	0.33	0.33
17.3	0.1	.40	.43	.42
17.7	0.0	.48	.52	.50
18.0	0.1	.54	.52	.53
18.3	0.1	.54	.52	.53
18.6	0.1	.50	.53	.50
19.2	0.0	....	....	.49
19.6	−0.1	....	....	.44
19.9	0.0	....	.66	....
20.1	0.0	.32	.63	.48
20.4	0.0	.56	.81	.68
20.7	0.0	.60	1.30	.93
20.9	0.1	.76	1.19	.94
21.1	0.1	.90	1.21	1.05
21.3	0.1	1.06	1.26	1.16
21.5	0.1	1.05	1.27	1.15
21.8	0.1	1.10	1.32	1.21
21.9	0.1	1.11	1.27	1.20
21.9	0.2	1.06	1.25	1.15
22.2	0.2	1.00	1.25	1.12
22.3	0.2	0.81	1.21	1.00
22.5	0.1	.84	1.22	1.02
22.7	0.1	.90	1.23	1.06
23.0	0.1	.87	1.11	.99
23.2	0.0	.87	1.11	.99
23.6	0.2	.86	1.00	.93
23.7	0.1	.78	1.05	.91
23.9	0.0	.91	.95	.93
23.9	0.2	.82	.96	.88
24.4	−0.1	....	....	.93

TABLE 4.—*Velocities V_ξ measured near the centerline in the reach 17<ξ<37 km*—Continued

$\bar{\xi}$ (km)	$\bar{\zeta}$ (km)	V_ξ (km/a)		
		t_0 to t_1	t_1 to t_2	t_0 to t_2
C. Photograph-overlay measurements (t_0=1978.297, t_1=1978.442, t_2=1978.576)—Continued				
24.8	0.2	....	....	.84
25.2	0.4	....	....	.72
25.4	0.4	....	....	.63
25.9	1.0	....	....	.42
26.4	1.0	.88	.70	.76
26.5	1.0	1.07	1.06	1.03
26.8	1.0	1.25	1.22	1.22
27.0	0.9	1.20	1.20	1.20
27.4	0.9	1.12	1.25	1.18
27.6	0.9	1.07	1.00	1.02
27.8	0.9	.65	.70	.68
28.1	0.9	.68	.70	.69
29.2	0.8	.66	.85	.70
29.5	0.7	.68	.98	.76
30.0	0.6	.87	1.14	.98
30.5	0.6	.92	1.19	1.02
30.9	0.5	.96	1.18	1.05
31.3	0.4	1.02	1.08	1.03
31.8	0.3	1.05	.98	1.02
32.2	0.2	1.03	1.08	1.05
32.6	0.0	1.12	1.01	1.05

existed constantly over that 102-day interval, would produce the 41 observed displacements.
Since

$$g(\xi)=v_\xi=\frac{d\xi}{dt}, \tag{2}$$

and since $g(\xi)$ is defined to be unchanging in time, by separating variables and integrating,

$$\int_{\xi_0}^{\xi_1}\frac{d\xi}{g(\xi)}=\int_{t_0}^{t_1} dt=t_1-t_0, \tag{3}$$

an integral condition is imposed on the velocity distribution for each trajectory. As established by Rasmussen (1983), individual points on $v_\xi=g(\xi)$ cannot be obtained directly from the observed displacements. Figure 14 shows a numerically constructed $1/g(\xi)$ using data for the 102-day interval; it is consistent through equation 3 with all trajectories in a best fit sense, but it is only one of infinitely many that can satisfy the integral condition.

Also shown in figure 14 are horizontal line segments from ξ_0 to ξ_1 with ordinate $(t_1-t_0)/(\xi_1-\xi_0)$, which represent the required integrals. The resulting centerline velocity $v_y=g(\xi)$ is shown in figure 15. The maximum difference between $g(\xi)$ and a velocity determined by a simple trajectory-average method is 21 percent for annual values and 3 percent for 102-day values (Rasmussen, 1983).

Transverse velocity profiles at ξ=17.8, ξ=21.8, and ξ=35.0 km derived from the 102-day interval data are listed in table 5 and shown in figure 16. Additional speed determinations in this reach are shown on plate 5.

The results shown in figures 14–16 apply only to the 102-day interval. Inspection of the shorter interval results (April 19 to June 11, and June 11 to July 30, 1978) indicates that velocities generally were lower than the 102-day average during the first interval, and higher during the second interval. Furthermore, the difference in velocity from the first to the second interval appears to depend on position (see, especially, fig. 16). Thus, a temporal fluctuation in velocity exists. To estimate the annual average speed, the results can be compared with three stakes in the reach that were measured over most (362 days) of the measurement year. The movement of stake 24 can be compared directly with the results shown in figures 14 and 15; its annual velocity was 13 percent higher than the 102-day average results. Stake 28.2 moved slightly slower than the 102-day points, but the stake was somewhat off the flow centerline. Stake 32 moved at about the same velocity as the 102-day

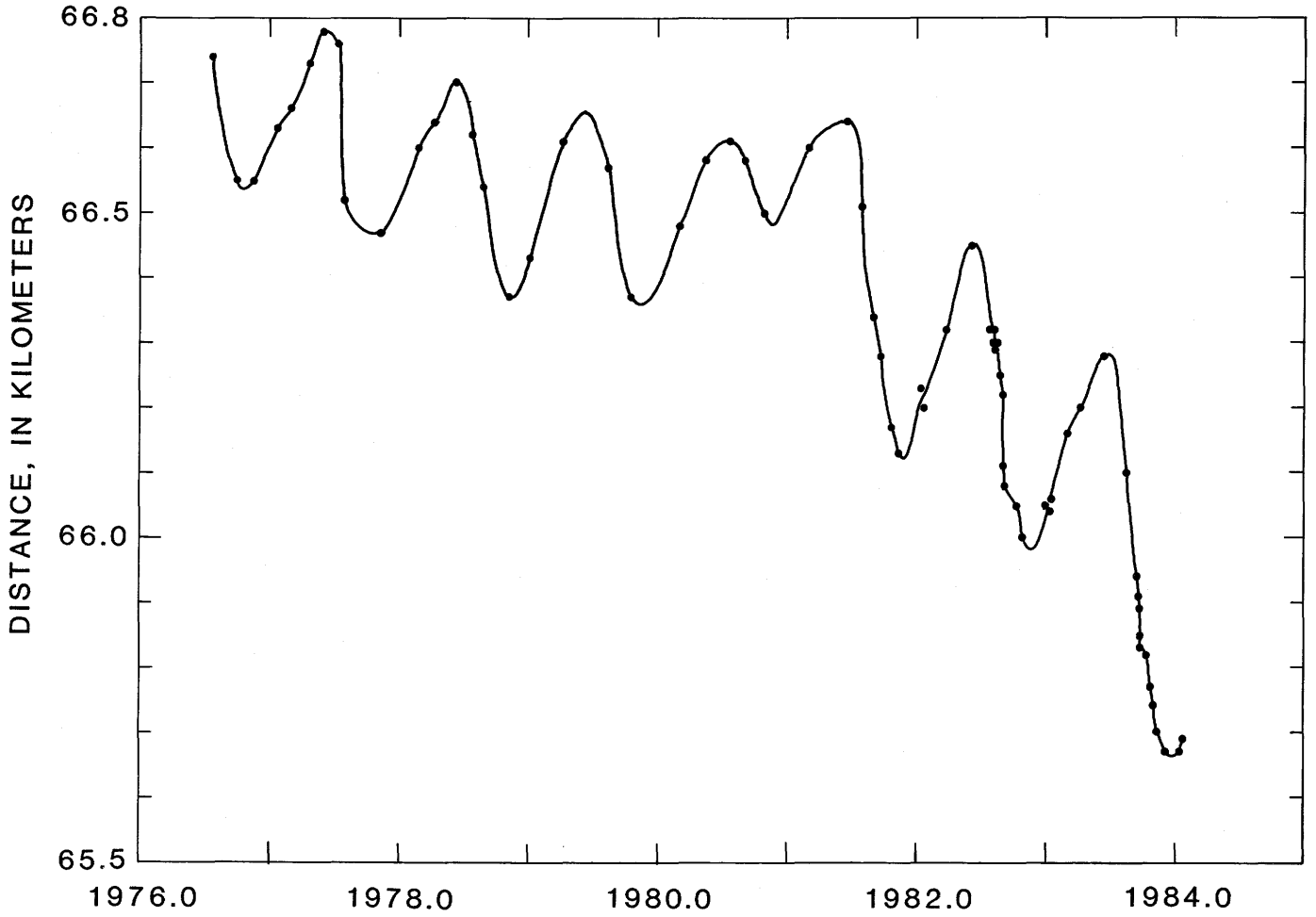

FIGURE 11.—Hand-drawn curve through width-averaged terminus position <Ξ> as a function of time for the flights 3–45 (table 2).

points, but the 102-day points are known with less accuracy in the region of stake 32 than in the vicinity of stake 24. Consequently, a correction factor to adjust the 102-day data cannot be determined with confidence. It is assumed that in the interval $17<\xi<25$ km, a multiplicative correction of 1.12 (or alternatively, an additive correction of 106 m/a) should be applied to the 102-day data in order to estimate the annual average. It is also assumed that, in the interval $28<\xi<37$ km, no correction should be applied. In the remaining interval, $25<\xi<28$ km, a correction should be applied that varies linearly with distance from 1.12 at $\xi=25$ km to 1.00 at $\xi=28$ km. Figure 13 and plate 5 show corrected results in this icefall reach.

Flow in this reach is characterized by high speeds (0.5–1.2 km/a) and extremely high rates of extension and compression. The longitudinal normal deformation rate $\dot{\epsilon}_{\xi\xi}$ is plotted in figure 15. The extension rate averaged over 100-meter intervals reaches 1 a^{-1} (extension being considered positive) at $\xi=20.4$ and 2 a^{-1} at 26.4 km, and the compression rate reaches -1.2 a^{-1} at $\xi=27.8$ km.

The two-dimensional deformation near $\xi=26$ km was investigated to determine the effect of this rapid longitudinal deformation on changes in thickness. Positions of five points that were in the form of a transversely elongated diamond shape were determined from vertical aerial photographs taken June 11 and July 30, 1978, as shown in table 6A. Coordinates of points were measured carefully on the photographs enlarged to a scale of 18,860, displacement comonents were determined, and their spatial gradients were calculated. The finite-strain formula,

$$\dot{\epsilon}_{\xi\xi}=\frac{1}{\Delta t}\ln\frac{\xi_{II}(1)-\xi_{II}(0)}{\xi_{I}(1)-\xi_{I}(0)}, \quad (4)$$

in which the subscripts I and II refer to two different points and (0) and (1) refer to their initial and final loca-

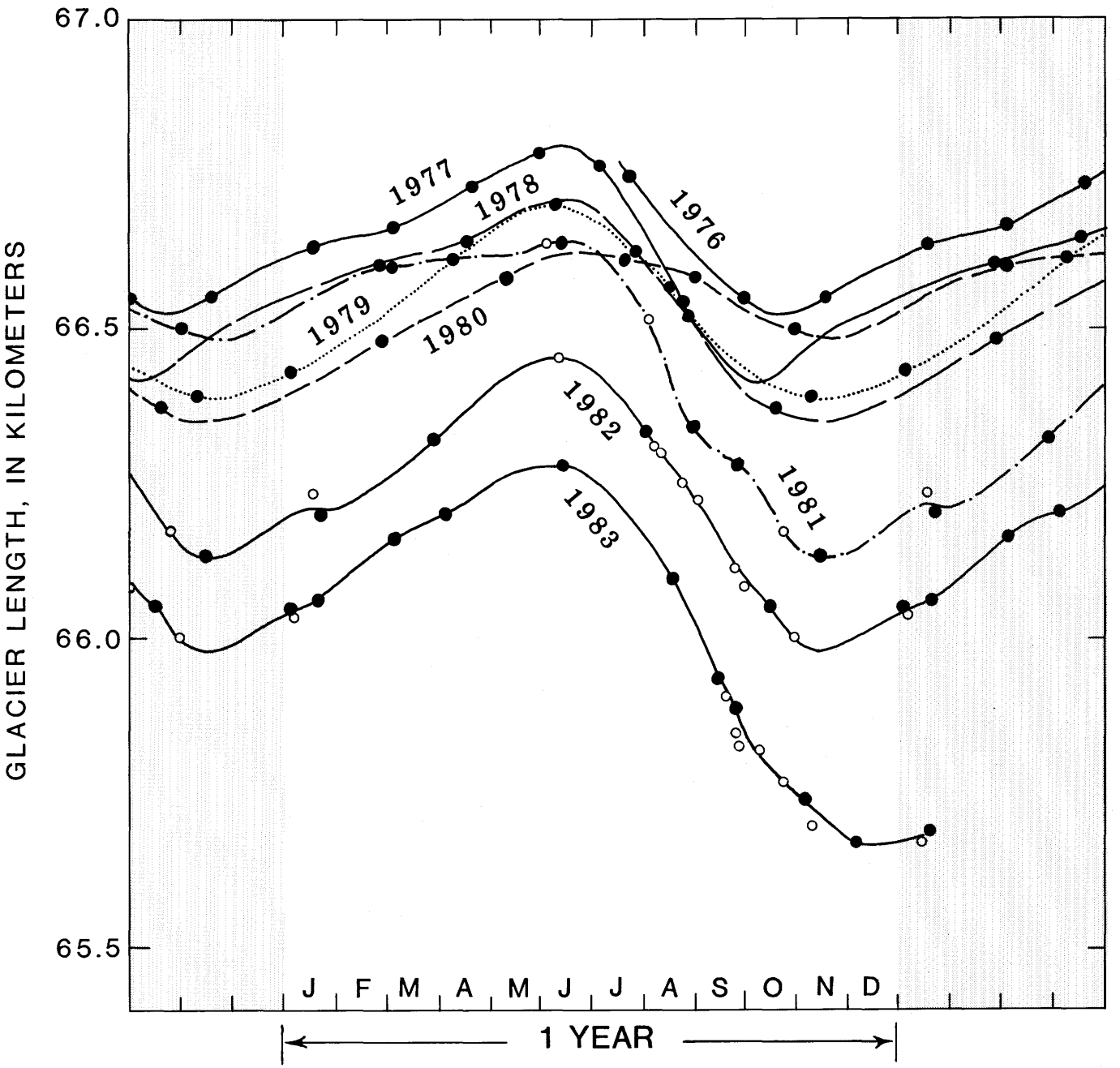

FIGURE 12.—Seasonal advance and retreat of Columbia Glacier for the years 1976–83, superimposed onto one year for comparison. The curves are repeated to either side in the gray areas to help visualize trends. Solid dots are data points obtained by photogrammetry (error is about 10 m), open circles are observations by less accurate methods (ship-borne radar, ground surveys), and the lines are smooth curves drawn through data points. Values are averaged over the width of the active terminus.

tions at times t_0 and t_1, was used. The formula yielded results that differed by a maximum of only 0.9 percent from those using simple spatial gradients. Gradients in the ξ-direction were calculated using points 1, 2, and 3, which lay approximately along the ξ-axis, and gradients in the ζ-direction using points a and c (table 6A). The principal components of the strain rate tensors at $\xi \approx 26.16$ and 26.46 km were calculated by standard methods and by assuming that the components are horizontal or vertical.

The results (table 6B) show that deformation is dominated by strong longitudinal extension, that this extension increases downglacier at a high rate (5.3×10^{-3} a^{-1} m^{-1}), and that there is also a slight transverse extension. The vertical strain rate is extreme (up to 2.55 a^{-1}, or 0.7 percent per day in compression).

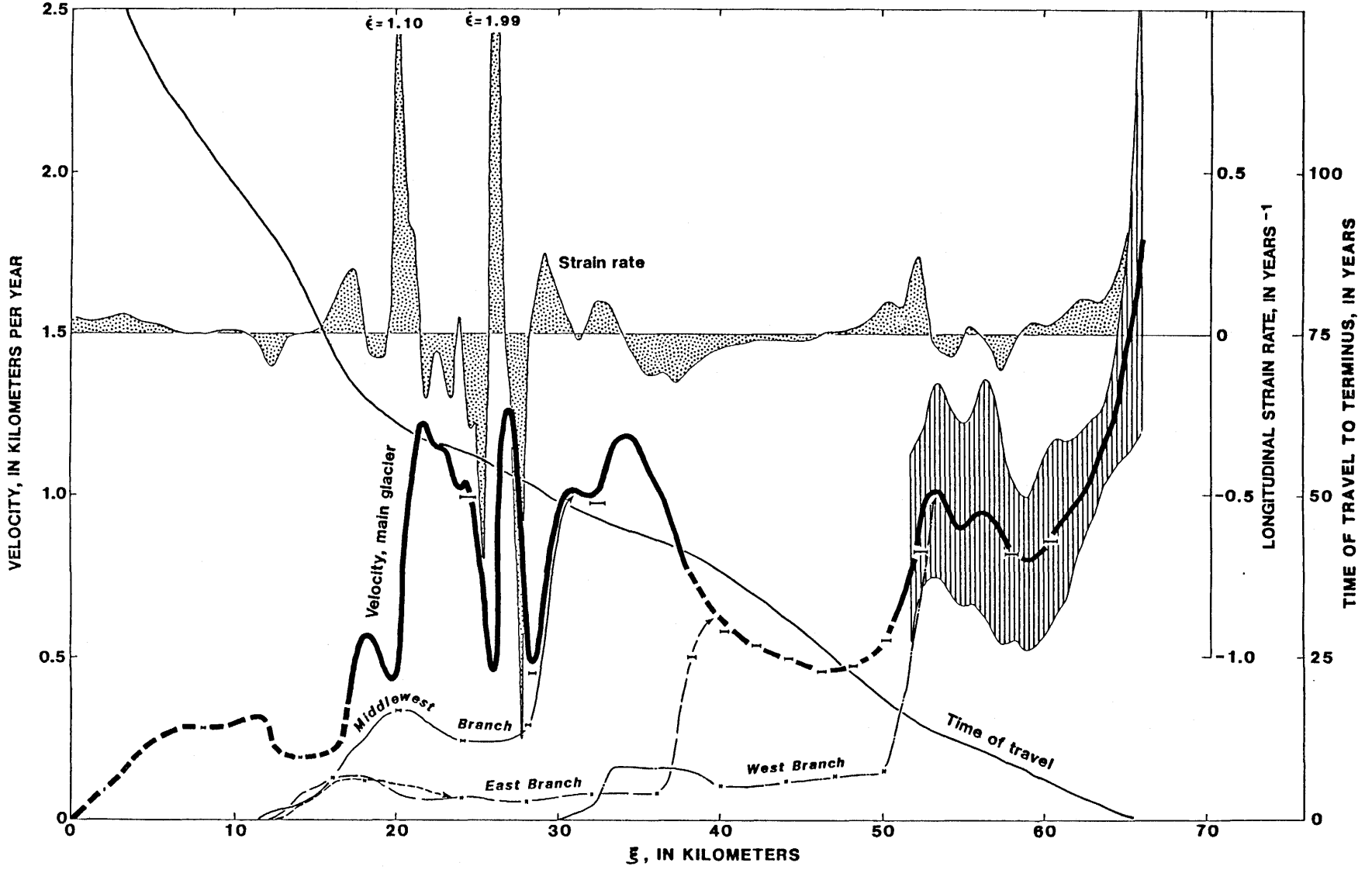

FIGURE 13.—Velocity along the centerline during the measurement year as a function of longitudinal distance for the main glacier (heavy) and its tributaries (light, dashed). For the main glacier, the time of travel to the terminus (light) and the longitudinal strain rate (stippled) are shown, as is the range of velocity variations with time in the lower reach (striped). Velocity values derived by stake surveys are shown as short lines indicating displacements during the year. Note: Stake at $\xi \approx 33$ km was not on exact centerline.

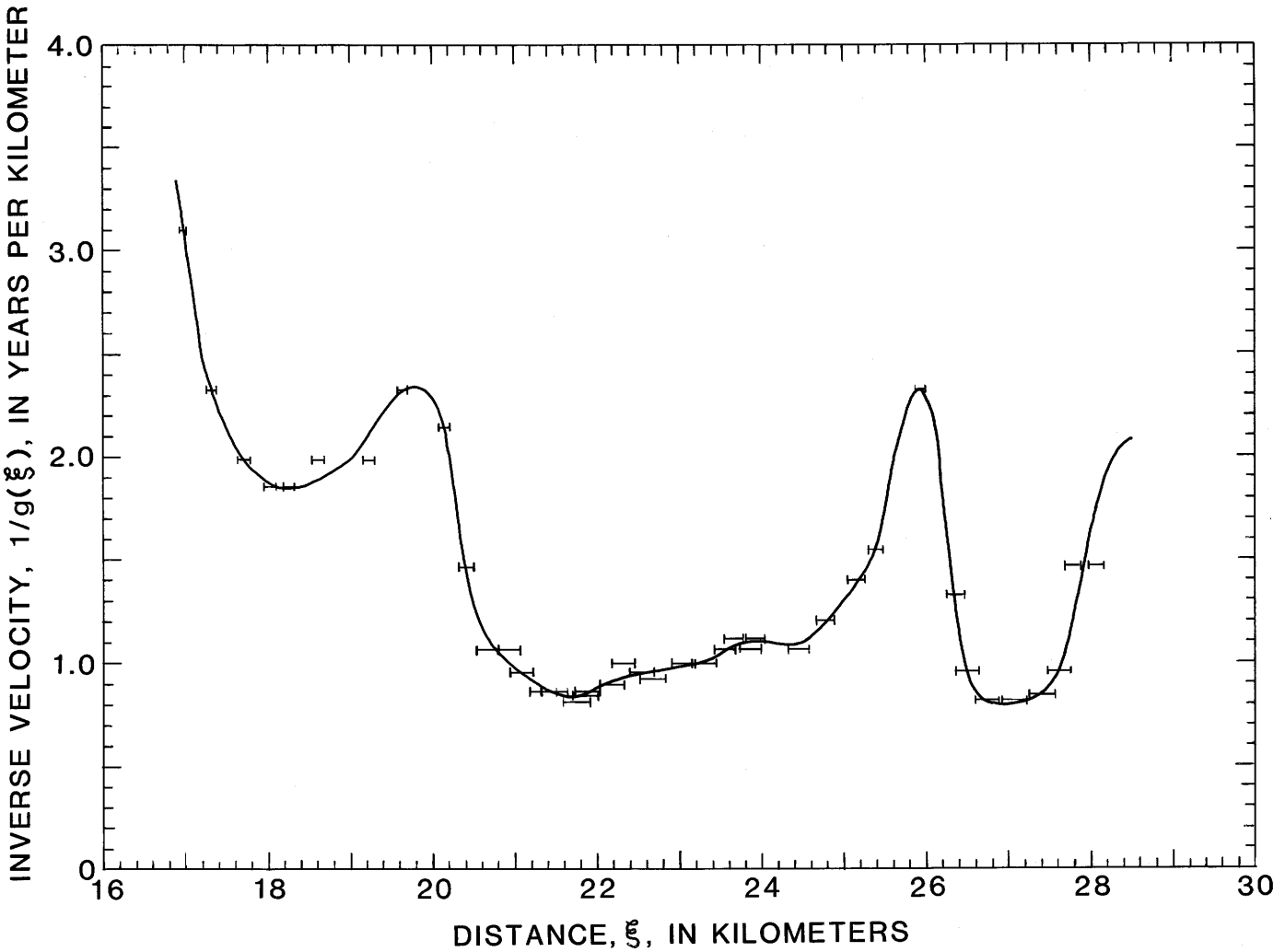

FIGURE 14.—Velocity-reciprocal function $1/g(\xi)$ in the icefall reach. The integral conditions (eq. 3) imposed by particle trajectory endpoints are also shown; they are met, in a least squares sense, by the curve.

These results have interesting implications with regard to the possible effect of vertical strain on mass-balance measurements. Conventional methods of measuring mass balance, using vertical measurements of snow-layer thickness at stakes, cores, or pits or on crevasse-walls, would be highly suspect unless the strain history of the snow column were known and the appropriate adjustment made. This would be difficult, because the strain near the surface in a block between two crevasses might be very different from the strain at depth.

These remarkable deformation rates given in table 6B also are evident in the crevasse pattern; figure 17 shows the glacier surface in the vicinity of $\xi=26$ km. The photograph reveals that crevasses begin as narrow cracks and, within only 300 m, enlarge to the point where the crevasse width exceeds the width of the block between crevasses (a stretching of 100 percent).

VELOCITY AND STRAIN RATE IN THE LOWER REACH

COORDINATE SYSTEMS AND THE GRIDDING OF DATA

Photogrammetric measurements determined a large number of displacements, but at points occurring irregularly in both space and time. Surface-velocity values obtained from the displacements were interpolated for aerial survey flights 2-30 onto a section of a 71×63 square data grid (i,j) positioned so that

$$\begin{pmatrix} i \\ j \end{pmatrix} = \frac{1}{\Delta} \begin{pmatrix} 65.65-y \\ 10.46+x \end{pmatrix}, \tag{5}$$

in which $\Delta=0.7625$ km is the grid spacing (fig. 1). The local x,y coordinate system is related to the geodetic

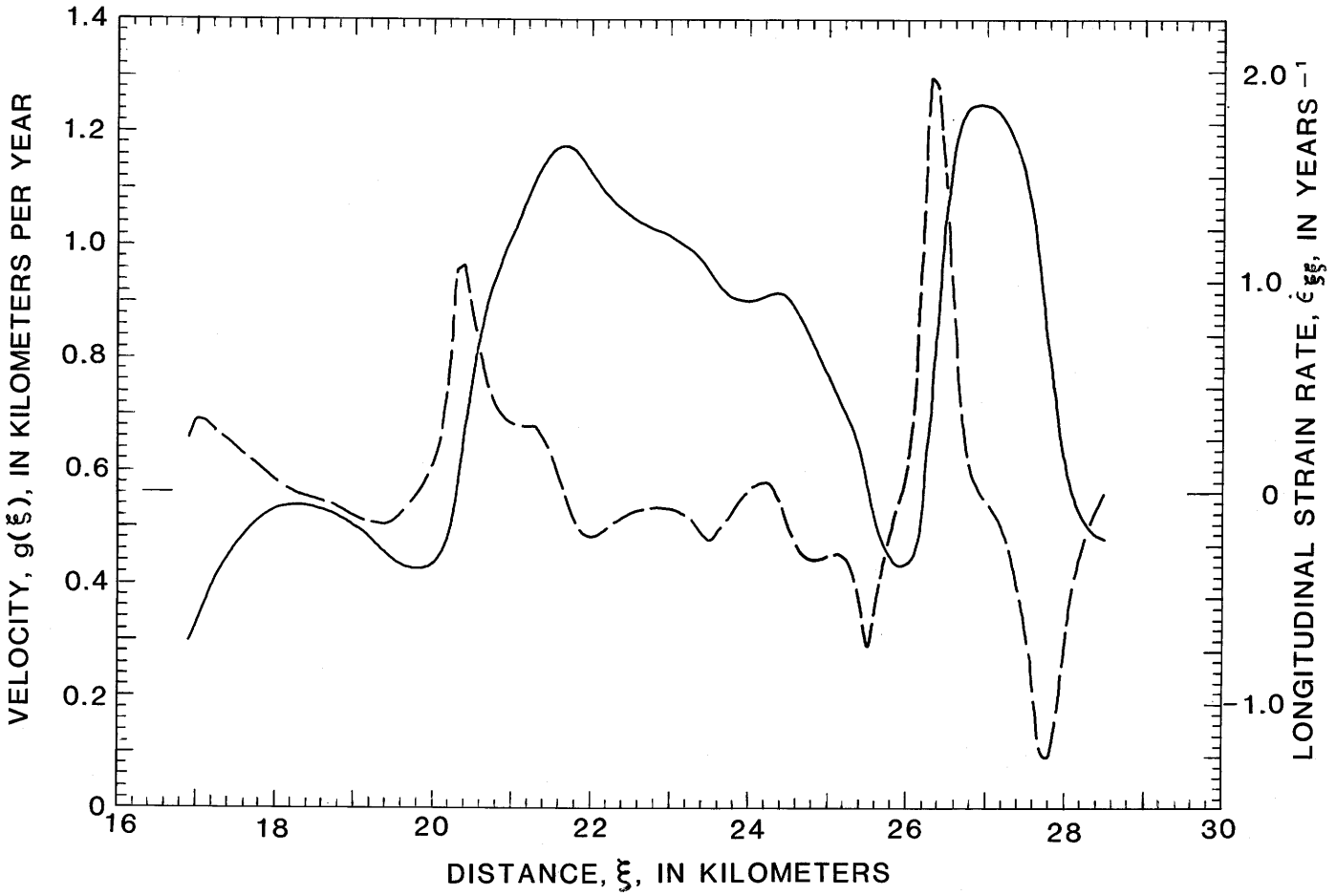

FIGURE 15.—Velocity function $V\xi=g(\xi)$ obtained as reciprocal of curve in figure 14 (solid). Also shown is its longitudinal strain rate (dashed).

UTM (Universal Transverse Mercator) system according to

$$\begin{pmatrix} x \\ y \end{pmatrix} = \frac{1}{0.9996} \begin{pmatrix} \text{UTM Easting} - 490 \\ \text{UTM Northing} - 6750 \end{pmatrix} \quad (6)$$

in which all variables are in kilometers. The interpolated x and y velocity components are u_{ij} and v_{ij}. Because they originated as flight-to-flight displacements, these components are themselves interflight average values. The measurement-year average values are obtained as the single, linear weighted average

$$\overline{u}_{ij} = \frac{1}{t_{17} - t_{11}} \sum_{L=11}^{16} (t_{L+1} - t_L)\, u_L, \quad (7)$$

in which u_L represents the value of u_{ij} between flights L and $L+1$, and similarly for $\overline{v}_{ij}$. Flights 11 and 17 are close to the beginning and the end of the measurement year, and $t_{17} - t_{11} = 0.991$ a.

SPATIAL DISTRIBUTION OF VELOCITY AND DEFORMATION

The measurement-year-averaged velocity for the lower reach is shown in plate 6 as velocity vectors at grid points and as scalar contours of the maximum velocity in a horizontal plane. Numerical values of the velocity components u,v (parallel to x,y) at grid points are listed in table 7. The velocity field is a typical one for a valley glacier, except at the terminus. Also, the observed values are larger than those normally observed in nonsurging mountain glaciers. The velocity increases as it enters a narrow "throat" at $\xi=52$ km, where it reaches 1 km/a. Below this throat, the velocity along the centerline decreases to about 0.8 km/a at $\xi=59$ km and then rises dramatically, exceeding 1.6 km/a near the terminus. The velocity at the exact terminus could not be determined because surface ice features were deforming

TABLE 5.—*Transverse profiles of velocity in the reach 17.8<ξ<35 km*

[Note that the velocities in the larger time interval do not necessarily equal the time-weighted average of velocities in the shorter time intervals because all three displacements were measured independently and the displacement vectors were not necessarily collinear. Some velocity values are missing because the point could not be identified on one or another of the photographs]

Point	Distance ξ (km)	Velocity (km/a)		
		April 19 to June 11	June 11 to July 30	April 19 to July 30
		At ξ=17.8 km		
SW margin	−1.62	0	0	0
1	−1.33	.15	.12	.14
2	−.99	.31	.28	.31
3	−.85	.35	.33	.35
4	−.54	.42	.45	.42
5	−.20	.44	.47	.48
6	.18	.49	.47	.50
7	.37	.48	.52	.51
8	.47	.49	.50	.50
9	.66	.44	.50	.47
10	.93	.31	.38	.35
11	1.09	.29	.29	.28
12	1.31	....	....	.14
NE margin	1.34	0	0	0
		At ξ=21.8 km		
W margin	−1.68	0	0	0
1	−1.62	....	.34	....
2	−1.50	.39	.61	.49
3	−1.31	.65	.90	.77
4	−1.13	.80	1.07	.92
5	−.94	.87	1.12	1.00
6	−.75	.95	1.18	1.05
7	−.61	.96	1.21	1.09
8	−.38	1.02	1.23	1.14
9	−.13	1.12	1.30	1.20
10	0	1.12	1.30	1.20
11	.22	1.08	1.28	1.17
12	.39	.92	1.18	1.03
13	.57	.75	1.01	.84
14	.73	.62	.85	.70
15	.93	....	.68	....
16	1.09	....	.61	....
E margin	1.32	0	0	0
		At ξ=35.0 km		
W margin	−1.95	0	0	0
1	−1.71	....	.29	....
2	−1.48	....	.64	....
3	−1.29	.96	.94	0.94
4	−1.09	1.06	1.04	1.04
5	−.20	....	1.21	....
6	0	1.13	1.19	1.16
7	.13	....	1.18	....
8	.30	1.02	1.16	1.09
9	.60	.99	....	....
10	.75	.95	.92	.93
11	.88	.89	....	....
12	.98	....	.66	....
13	1.09	.73	....	....
E margin	1.33	0	0	0

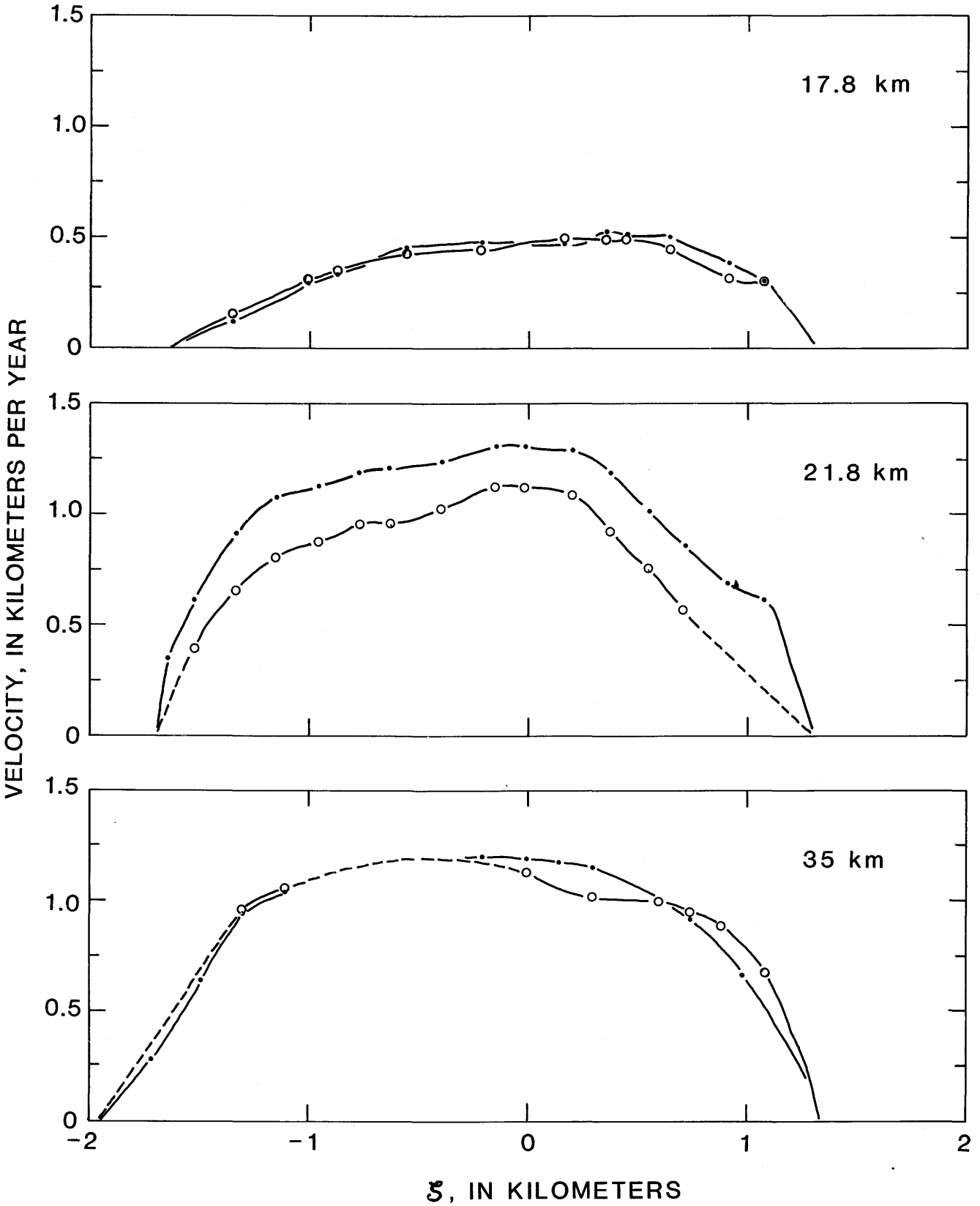

FIGURE 16.—Transverse velocity profiles for ξ=17.8, ξ=21.8, and ξ=35.0 km for April 19 to June 11, 1978 (circles), and for June 11 to July 30, 1978 (dots), illustrating data of table 5.

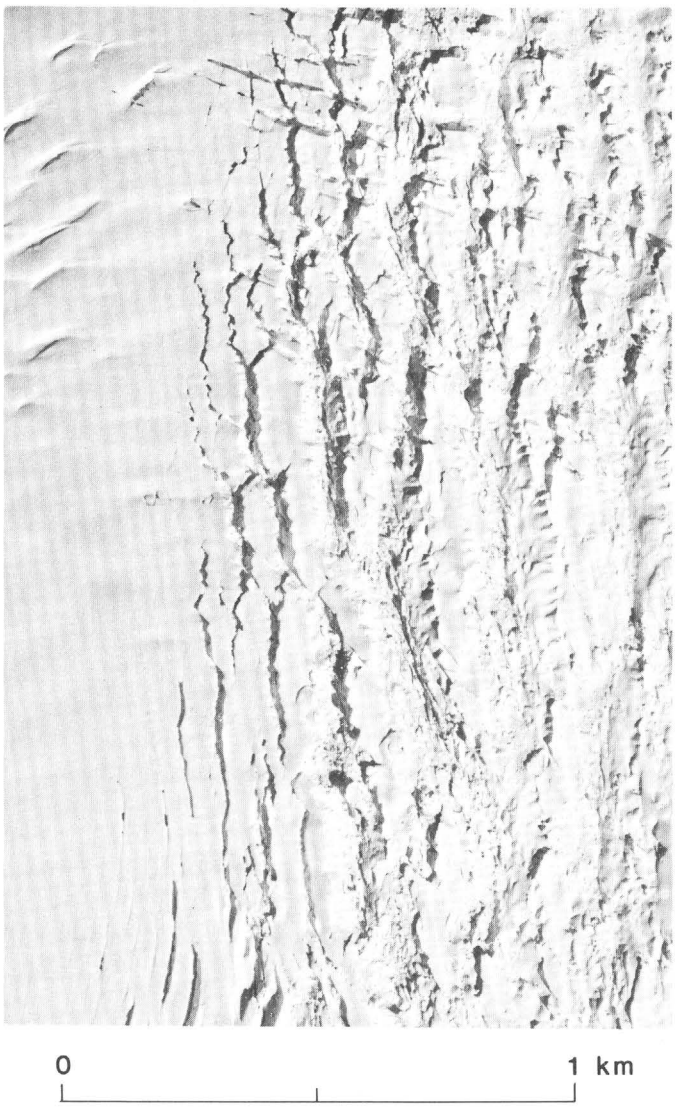

FIGURE 17.—Vertical aerial photograph of the main glacier in the vicinity of ξ=26 km, April 29, 1978, showing marked increase in crevasse width over a short distance due to intense extension. The glacier flows to the right (south).

rapidly and usually could not be tracked from one aerial photographic survey flight to the next. Furthermore, the terminus position changed during the measurement year. The transverse pattern of velocity is that normally expected for a valley glacier. Although this glacier moves rapidly, there is a smooth decrease of velocity from centerline to margin and no indication of abrupt shear at the margins (Block–Schollen flow) as described by Finsterwalder (1938).

The strain-rate field can be obtained from the spatial derivatives of the velocity field. The measurement-year-averaged strain-rate field for the lower reach is portrayed on plate 7 by showing the principal axes of the strain-rate tensor, and the trajectories of greatest (most extending) and least (most compressing) strain rates. The strain-rate field clearly shows extension toward the throat at $50<\xi<52$ km, accompanied by an arched pattern of compression.

At ξ=52 km the pattern abruptly changes to a typical splaying pattern dominated by shear near the margins and a slight transverse extension. At the point of change there occurs an isotropic, singular point—a lemon (Thorndike and others, 1978; Nye, 1981, 1983). Farther down the glacier, at ξ=59 km, the pattern changes to longitudinal extension, and at that point there is another isotropic point—a star. These isotropic points characterize the structure of the velocity field. The points are structurally stable in that they cannot be annihilated by a small change in conditions but can only be moved slightly. Interestingly, no monstars—a type of isotropic point generally expected to occur in glaciers (Nye, 1983)—occur in this field.

Near the terminus, a strong pattern—an arch of compression combined with extension toward the calving front—develops. The compressional arch, however, is not as fully developed or as clearly related to calving for these data averaged over a year as it is when data from shorter time intervals are examined.

CHANGES IN VELOCITY AND STRAIN RATE WITH TIME

The surface velocity is a vector function of three independent coordinates x,y,t and is difficult to analyze in all three dimensions. The dimensionality is reduced by considering only the greatest value of the dominant component across each grid row. The flow is almost southerly in the lower reach, so the dominant flow component is v, and the magnitude of the greatest value across a row is denoted V.

For any particular row, for each of the 21 intervals between successive flight dates t_9, t_{10}, ..., t_{30} (table 1), the time-averaged V_L (Fountain, 1982) are denoted V_9, V_{10}, ..., V_{29}. Figure 18 shows a continuous $V(t)$ for row i=60 obtained from the V_L values. Points on a pseudotrajectory (t_L, Y_L) are formed by integrating the V_L with respect to t,

$$Y_L=Y_{L-1}+(t_L-t_{L-1})V_{L-1}, \tag{8}$$

in which, arbitrarily, Y_9=0. Also the (t_L,Y_L) are shown for row i=60 (fig. 18). The derivative $df(t)/dt$ of any increasing, differentiable function $f(t)$ constrained to pass through the (t_L, Y_L) is a velocity function $V(t)$ that has the same time-averaged values as the V_L.

The class of functions chosen for $f(t)$ is the well-known cubic splines of zero deficiency. On each interval (t_L, t_{L+1}) the spline is a separate cubic polynomial in t, and at each t_L it is continuous in function value and first two

TABLE 6.—*Coordinates of points and components of the strain-rate tensor, for two locations near ξ=26 km*

[Subscripts 0 and 1 on coordinates refer to positions of points on June 11 and July 30, 1978, respectively. Tensor components $\dot{\epsilon}_1$ and $\dot{\epsilon}_2$ are the greatest and least horizontal principal components, $\dot{\epsilon}_3$ is the vertical principal component (extension is considered positive), and θ is the angle between $\dot{\epsilon}_1$ and the ξ-axis]

A. Point coordinates

Point	ξ_0 (km)	ξ_1 (km)	ζ_0 (km)	ζ_1 (km)
1	25.922	25.970	1.008	1.039
2	26.327	26.148	1.004	1.017
3	26.466	26.609	0.979	0.982
a.	26.385	26.475	−0.834	−0.881
c.	26.479	26.555	2.196	2.219

B. Strain-rate tensor components

ξ (km)	ζ (km)	$\dot{\epsilon}_1$ (a^{-1})	$\dot{\epsilon}_2$ (a^{-1})	$\dot{\epsilon}_3$ (a^{-1})	θ (°)
26.16	1.02	0.80	0.15	−0.95	10.1
26.46	1.00	2.40	0.15	−2.55	5.0

derivatives. Its derivative function, $V(t)$, is a quadratic spline of zero deficiency (Rasmussen, 1982); on each interval it is a separate quadratic polynomial in t, and at each t_L the quadratic spline is continuous in function value and first derivative. A cubic spline is not determined solely by the points through which it must pass; it requires two boundary conditions. The boundary conditions usually are imposed in the form of derivative conditions at the endpoints. In this application, the derivatives of the cubic spline at t_9 and t_{30} are the velocities $V(t_9)$ and $V(t_{30})$.

The effect on $V(t)$ of the end condition imposed at t_9 or t_{30} oscillates in sign and decays rapidly. The effect of an increment to the endpoint value never exceeds 9 percent of that increment except within three flights from that end (i.e., flights 9–12 or 27–30) and never exceeds 1 percent except within four flights (i.e., flights 9–13 or 26–30). Thus, between flights 13 and 26, the obtained $V(t)$ is almost unaffected by the endpoint values because the spline method is insensitive during that interval to its boundary conditions. This does not mean that the obtained $V(t)$ exactly represents the actual velocity distribution during that interval, because there are an infinite number of $V(t)$, of various classes of functions, that satisfy the integral conditions.

The general source of the $V(t_9)$ and $V(t_{30})$ boundary conditions was the $V(t)$ character of the spline fits in the interior of the $[t_9, t_{30}]$ interval. The quasi-periodic $V(t)$ curves were simply extended from the interior of the interval—where the cubic splines are nearly unaffected by their boundary conditions—to give values of V_9 and V_{30}. Other particular sources of boundary condition information were: photogrammetrically determined velocities for $t<t_9$ and $\xi>62$ km (Fountain, 1982), photograph-overlay velocities for $t>t_{30}$ and $\xi\geq 64$ km (Austin Post, written commun., 1982), and stake survey velocities for $t>t_{30}$ at ξ=60 km (L. R. Mayo, written commun., 1982). The boundary conditions at both t_9 and t_{30} were then smoothed slightly in the y-direction to ensure that $V(y,t_9)$ and $V(y,t_{30})$ were free of spurious features not implied by $V(y,t)$ for t in the interior of the $[t_9, t_{30}]$ interval. The cubic and quadratic spline approximations to $Y(t)$ and $V(t)$ for ξ=59 km are shown in figure 18.

Figure 19 shows $V)(y,t)$ for the lower reach, as derived by the contouring in space and time of the 19 $V(t)$ curves for rows 51 through 69. The contouring was done with the CalComp General Purpose Contour Program. The plot shows relatively high speeds at $53<i<57$ ($53<\xi<57$ km), due to convergence into the throat (pl. 6), and near the terminus (i=69, ξ=66 km). Generally, high speeds occur in late spring (0.35 a after the beginning of each year) and low speeds in late summer (0.70 a after the beginning of each year). In addition, high speeds occur at the terminus at 1977.80, 1978.85, and 1979.95, but not in 1980; another maximum begins to appear in late 1981. These maxima at the terminus die out upglacier and appear to be gone above i=59 (ξ=58 km).

Much of the structure in figure 19 is due to the way the cross-sectional area changes with distance y. This effect can be eliminated by normalizing the velocity at each row by dividing by the long-term average velocity:

$$\hat{V}(y,t)=v(y,t)/\left[\frac{1}{t_{30}-t_9}\int_{t_9}^{t_{30}} V(y,t)dt\right]. \qquad (9)$$

The variation in normalized velocity $\hat{V}(y,t)$, shown in figure 20, is simpler than that of $V(y,t)$. Figure 20 shows the main structures of high speeds in late spring and low speeds in late summer, and pulses of high velocity near the terminus that die out upglacier, as in figure 19. Figure 20 clearly shows that the velocity pulses near the terminus propagate upglacier as they diffuse.

In the lower reach, the ice thickness h is of the order of 500 m, and the surface slope α is about 0.025 (Rasmussen and Meier, 1982). Seasonal changes due to mass balance alone (assuming no compensating changes in the emergence velocity) might change the thickness by the order of 5 m and the slope by about 0.0005. The flow of a temperate glacier is a combination of flow by internal deformation V_d and flow by basal sliding V_b. For simple laminar flow, V_d is proportional to $\alpha^n h^{n+1}$ where

TABLE 7.—*Measurement-year average values (m/a) of velocity components u and v on indicated section of 0.7625-kilometer grid*

[Values are formed as simple time-interval-weighted average of data in Fountain, 1982 (tables 6, 7)]

Grid row No.	Grid column No.							
	19	20	21	22	23	24	25	26
	A. Velocity component *u* (positive to the east)							
51	70	35	−51	−240	−365	−294	0	0
52	26	77	87	24	−84	−131	0	0
53	34	86	156	198	123	24	0	0
54	0	−22	−46	67	133	0	0	0
55	−100	−163	−161	−23	120	106	0	0
56	−66	−116	−55	66	134	107	0	0
57	−15	26	131	211	212	129	44	0
58	10	121	269	313	288	185	73	0
59	0	154	334	311	282	233	135	0
60	0	127	261	273	248	226	144	41
61	0	68	195	223	222	218	152	27
62	0	−99	81	170	190	182	137	49
63	0	−114	−16	110	117	103	78	30
64	0	−87	−14	35	11	10	16	−4
65	0	0	17	−19	−92	−109	−84	−36
66	0	0	−12	−94	−163	−197	−180	−17
67	0	0	−73	−247	−249	−291	−202	−20
68	0	0	−250	−314	−359	−333	−133	0
69	0	0	0	−495	−489	−395	−24	0
	B. Velocity component *v* (positive to north, values given are negative)							
51	162	433	723	753	507	194	0	0
52	119	519	873	930	661	180	0	0
53	98	595	988	995	650	124	0	0
54	0	644	897	951	662	0	0	0
55	144	588	873	912	710	252	0	0
56	165	685	916	930	797	418	0	0
57	158	629	898	876	740	426	97	0
58	111	527	819	817	747	485	157	0
59	0	427	728	791	766	636	335	0
60	0	301	663	740	760	741	481	115
61	0	235	557	703	798	869	636	132
62	0	107	421	695	830	882	719	254
63	0	100	327	697	856	921	787	307
64	0	60	224	680	887	988	860	342
65	0	0	175	697	974	1,081	930	272
66	0	0	173	802	1,086	1,141	874	148
67	0	0	290	1,088	1,271	1,255	729	118
68	0	0	417	1,237	1,534	1,356	427	0
69	0	0	0	1,658	1,759	1,163	227	0

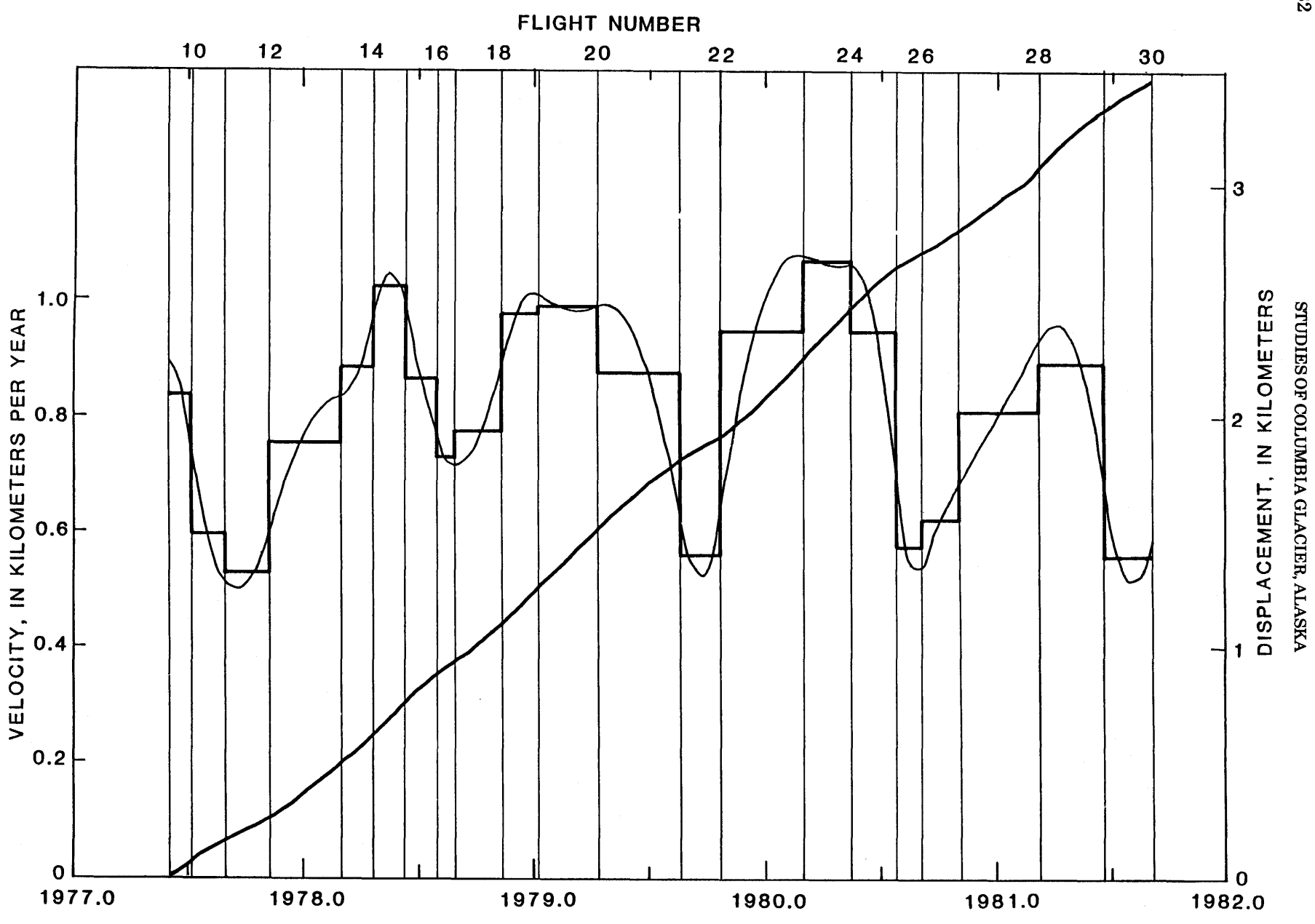

FIGURE 18.—Cubic spline (heavy) through pseudotrajectory points (eq. 8, scale at right) and the quadratic spline velocity function (light, scale at left) obtained from it, for row i=60, over the period June 2, 1977 through September 1, 1981 (flights 9 through 30). Also shown (step function) are the average velocity values V_L between successive flight dates.

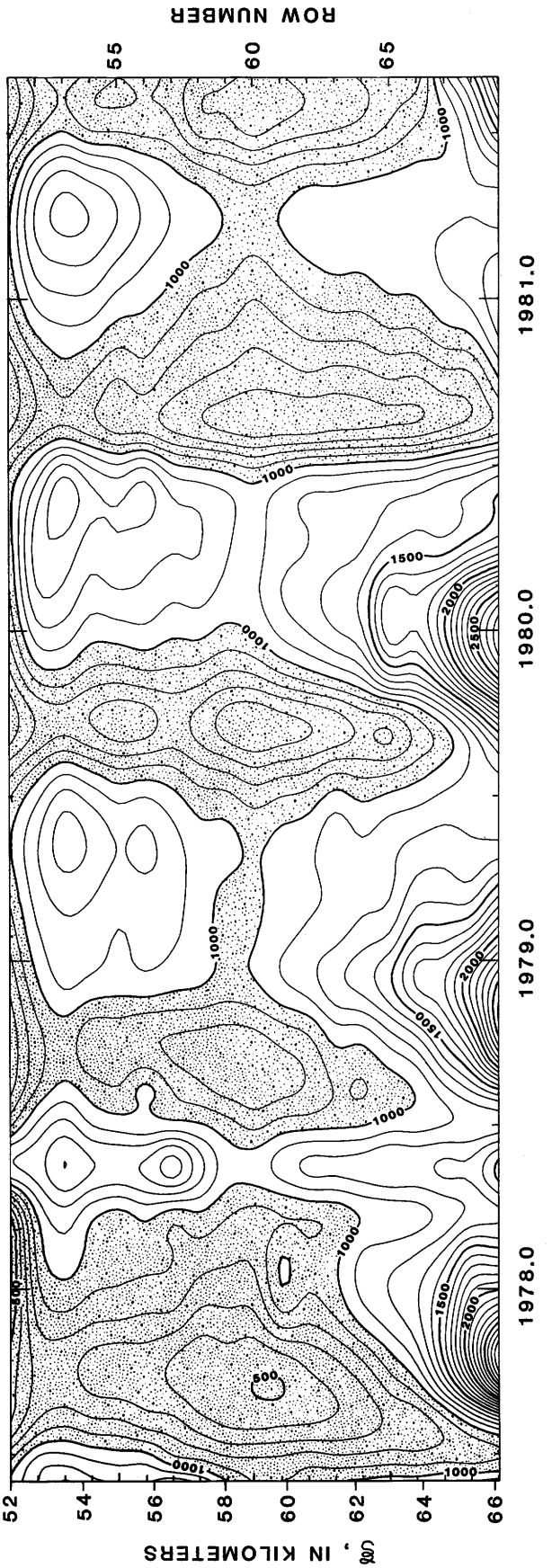

FIGURE 19.—Velocity (m/a) as a function of longitudinal distance ξ and time t.

$n \approx 3$ (Nye, 1952; Paterson, 1981). Thus, the seasonal change from a thicker, flatter glacier in spring to a thinner, steeper glacier in fall would cause a change in V_d of only about 2 percent. The seasonal changes shown in figures 19 and 20 are much larger than this, so they must be accounted for by changes in sliding.

A lower bound estimate of V_b can be made by assuming that all the seasonal variation in surface velocity is produced by changes in the sliding velocity. If V_d is approximated by min $V(y,t)$, defined as the minimum velocity observed over the interval $t_9 \le t \le t_{30}$, then

$$V_b^*(y,t) = V(y,t) - \min V(y,t) \tag{10}$$

gives that lower bound estimate, which is less than $V_b(y,t)$ by a constant, but unknown, amount. If it is normalized, by dividing by the total velocity, then

$$\lambda^* = 1 - \frac{\min \hat{V}(y,t)}{\hat{V}(y,t)} \tag{11}$$

is a lower bound estimate of the sliding fraction. The variation of the lower bound estimate with time and distance (fig. 21) is similar to the variation of $\hat{V}$. The same pattern of seasonal accelerations and decelerations occurs, as does the propagation and diffusion of velocity pulses originating at the terminus. Exclusive of the terminus pulses, the times of maxima and minima in V and λ^* taken from figures 20 and 21 are listed in table 8.

The seasonal fluctuations in velocity are remarkably synchronous from year to year, and the timing of maxima and minima in $\hat{V}$ and λ^* are nearly identical. Maximum velocity is reached at 0.33±0.05 a (corresponding to April 29±19 days), and the minimum at 0.69±0.05 a (corresponding to September 9±19 days). There is no evidence of changes in timing with distance, such as by the propagation of a wave. If these maxima and minima propagate downglacier, the wave speed must be higher than about 200 km/a. Thus, one is led to the conclusion that velocity maxima and minima are caused by maxima and minima in sliding occurring simultaneously over the lower reach and probably are caused by changes in the pressure or thickness of subglacial water (Weertman, 1972; Hodge, 1974; Bindschadler, 1983; Iken and others, 1983). Another interpretation, suggested by Lliboutry and Reynaud (1981), is that a constriction, such as that at ξ=52 km, controls the velocity fluctuation below that point.

The pulse of velocity that originates near the terminus can be explained by comparing fluctuations of velocity near the terminus with variations in the length of the glacier (fig. 22). The graph in figure 22 shows a quadratic spline fit for $V(t)$ at i=69 ($\xi \approx 66$ km) and the observed length of the glacier at times of aerial photographic survey flights (figs. 11, 12).

TABLE 8.—*Times of maxima and minima in velocity of the lower reach*

Maxima					
$\hat{V}$	1978.38	1979.34	1980.35	1981.25	
λ^*	1978.38	1979.34	1980.35	1981.25	
Minima					
$\hat{V}$	1977.73	1978.72	1979.73	1980.67	1981.61
λ^*	1977.74	1978.73	1979.72	1980.65	1981.60

The two curves in figure 22 correlate remarkably well in a negative sense; that is, glacier retreat correlates with velocity acceleration and advance correlates with deceleration. In fact, the curves between measurement points could be altered to improve the apparent correlation even further. Pronounced velocity maxima occur at 1976.84, 1977.77, 1978.83, 1979.97, and 1981.87, and a very weak velocity maximum occurs at about 1981.0. Thus, the mean time is 0.88±0.09 a (November 17±32 days). Retreat causes an increase in the effective slope near the terminus and a decrease in the longitudinal compressive stress; therefore, acceleration in ice velocity would be expected.

The change in length of an iceberg-calving glacier depends on the difference between iceflow and calving,

$$\langle \dot{\Xi} \rangle = \langle V_e \rangle - \langle V_c \rangle \tag{12}$$

where $\langle \dot{\Xi} \rangle$ is the rate of change in length, $\langle V_e \rangle$ is the ice velocity at the terminus, and $\langle V_c \rangle$ is the calving speed (calving discharge divided by cross-section area of the terminus), and all quantities are averaged over the width (Meier and others, 1980; Rasmussen and Meier, 1982).

The width-averaged velocity at the terminus is not known. During the period June 2, 1977, to September 1, 1981, the terminus varied in position between $66.348 < \xi < 66.775$ km; centerline velocity V_{66} was measured at ξ=66 km during the same period. It might be supposed that $\langle V_e \rangle$ could be calculated from V_{66}, by using the assumptions that the discharge does not change appreciably over this short distance during any given time interval and that the relation between centerline and width-averaged velocities are known at all times at both ξ=66 and at the terminus. The first assumption probably is valid, but the thickness distribution is not well known; few radio-echo sounding results for the bed altitude were obtained in this interval, and the ice-surface altitude was measured only twice and was known to

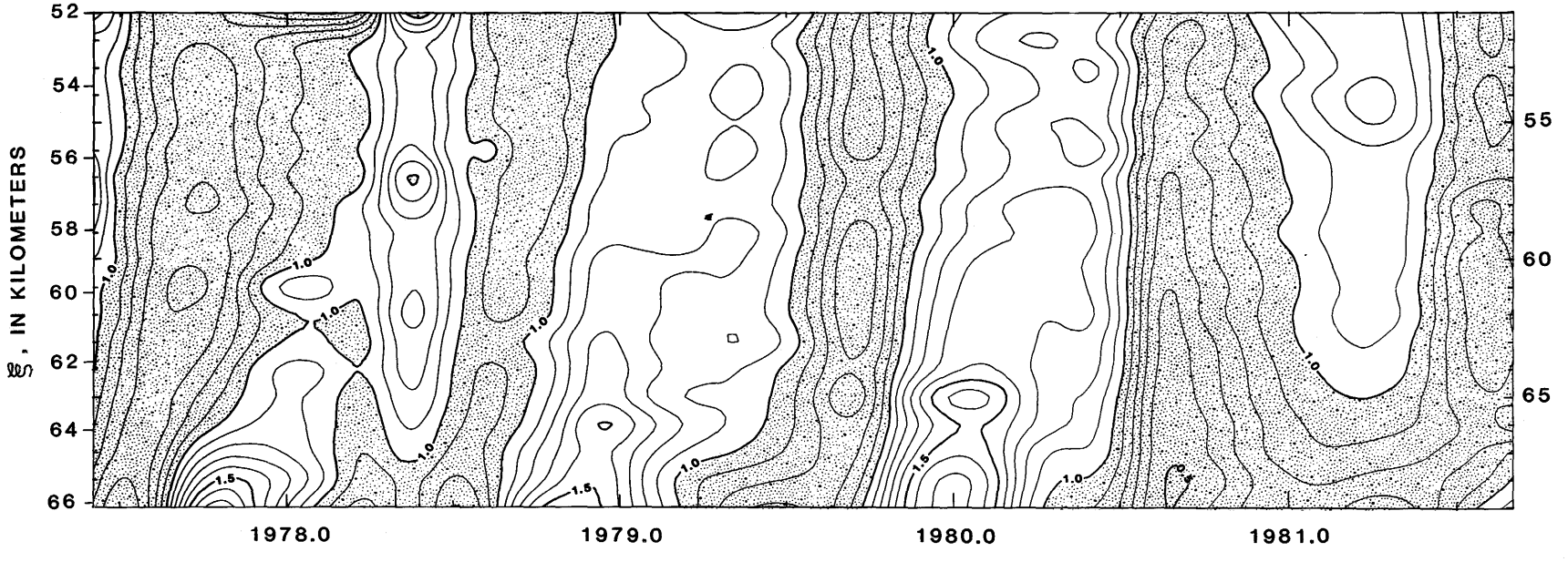

FIGURE 20.—Normalized velocity as a function of longitudinal distance ξ and time t, obtained from figure 19 by dividing by the average value over the entire time period (eq. 9).

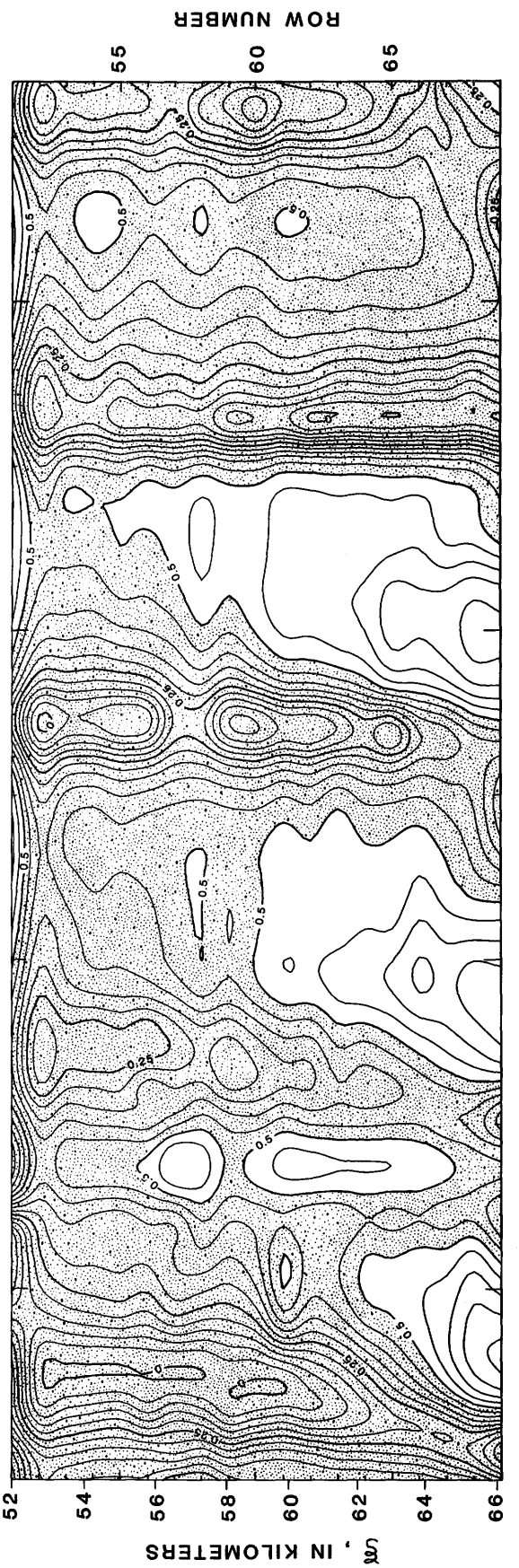

FIGURE 21.—Lower bound estimate of fraction of velocity that is due to sliding (eq. 11), as a function of longitudinal distance ξ and time t.

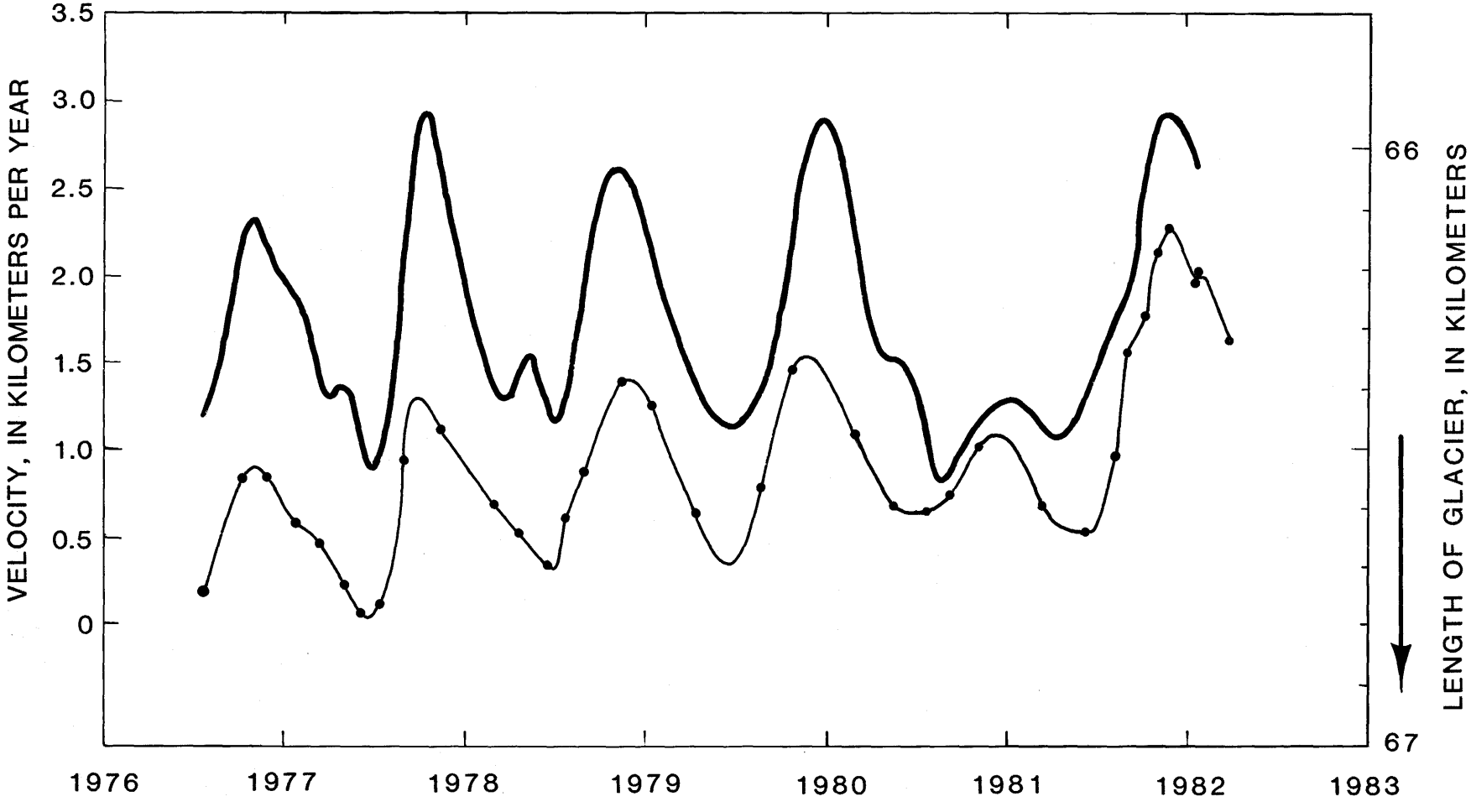

FIGURE 22.—Velocity (m/a) at ξ=66 km as a spline fit to interflight average values (heavy) and a hand-drawn curve (light) through terminus positions (dots) at time of photography flight. Note: Velocity curve was derived from a spline fit during the interval June 2, 1977, to September 1,1981; this curve was extended at both ends by drawing a smooth curve through additional velocity values obtained at the terminus.

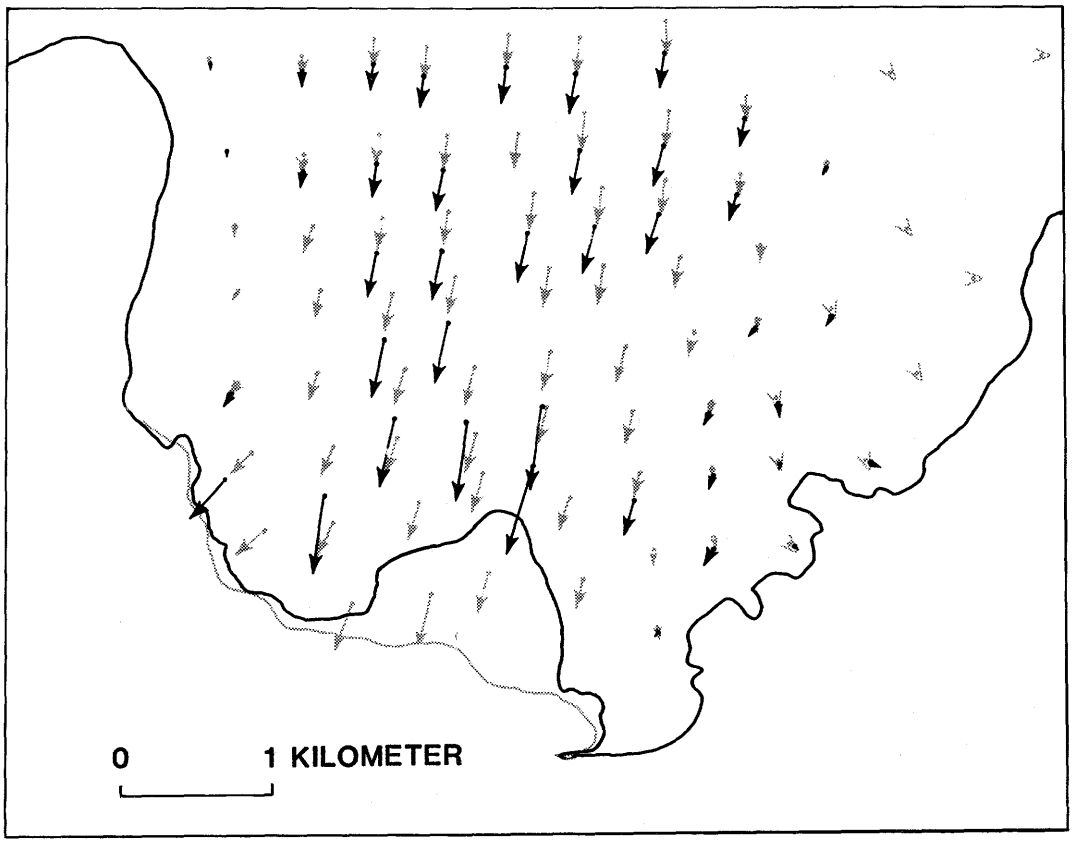

FIGURE 23.—Terminus configuration on June 2, 1977 (light), and on August 29, 1977 (heavy), combined with average velocity vectors for June 2 through July 7, 1977 (light), and for August 29 through November 8, 1977 (heavy), demonstrating acceleration and convergence induced in velocity field by embayments. Vector lengths represent 100-day displacements. Open arrows indicate flow direction where actual vectors are too small to show.

change with time. The second assumption clearly is invalid: $V_{66}(\zeta)$ was not measured, and $V_e(\zeta)$ varied with time as embayments formed and filled. Thus, equation 12 cannot be used to calculated V_c accurately, especially its variation with time, without additional information.

There is a strong seasonal variation in V_c, presumably because V_c has a relation to subglacial runoff (Sikonia and Post 1980; Sikonia, 1982). Calving also increases with increasing water depth (Brown and others, 1982) or with a decrease in the ice thickness unsupported by buoyancy (Sikonia, 1982), which decreases as water depth increases. In midsummer, runoff is high and V_c is also high, causing rapid retreat; in late summer and fall, runoff decreases but V_c is still high because retreat has placed the terminus in deeper water (pl. 3).

CHANGES IN VELOCITY AND STRAIN RATE NEAR THE TERMINUS

Variations of speed with time near the terminus have been discussed and portrayed in figures 19–22. Changes in the pattern of the velocity field and its spatial derivative, the strain-rate field, are discussed in this section.

Seasonal changes in calving cause seasonal changes in the terminus configuration. In the summers of 1976–79, rapid calving in a restricted portion of the terminus led to the formation of deep embayments. Figure 23 shows a typical no-embayment velocity field contrasted with a typical velocity field at the time of a large embayment. After formation of an embayment, the velocity vectors converge toward the embayment and the acceleration increases toward the embayment. Thus, the velocity field is sensitive in at least two dimensions to changes in terminus configuration.

It is interesting to note that the final configuration of a large embayment, such as the embayments formed in 1976–78, parallels closely a trajectory of most compressive principal strain rate (fig. 24). Thus, the embayment appears to interact with the velocity field to develop an

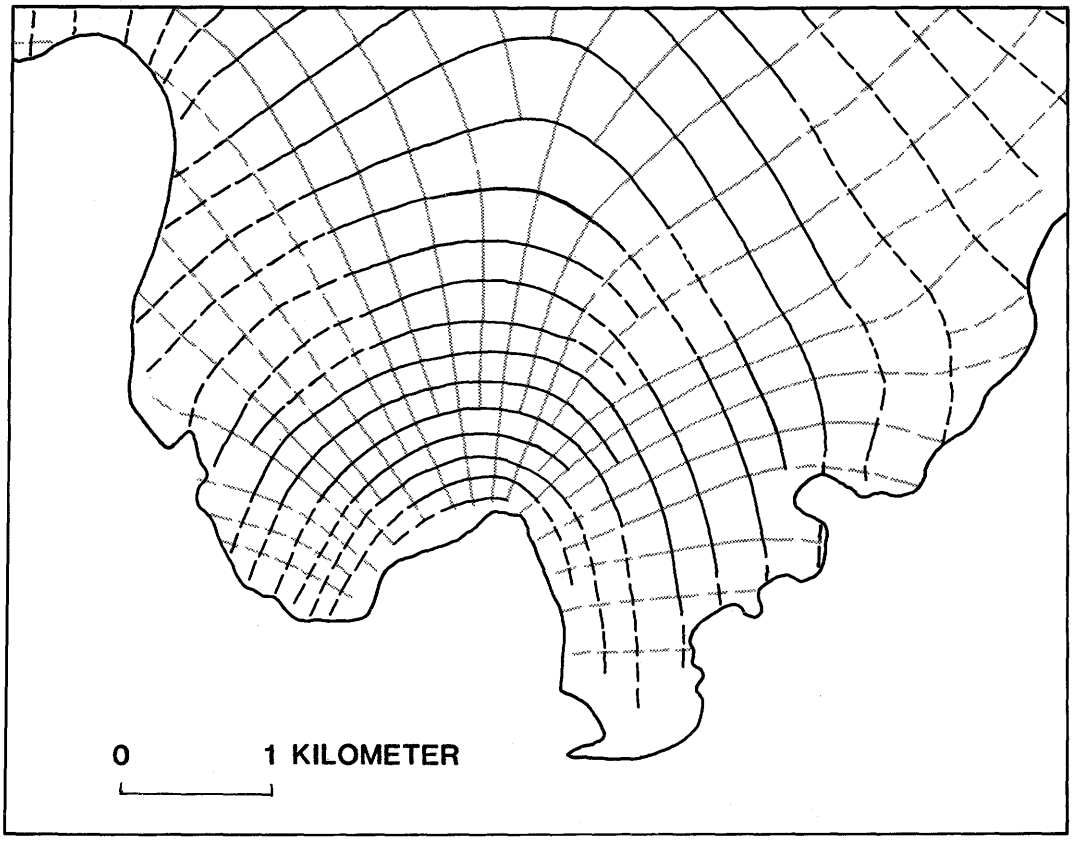

FIGURE 24.—Trajectories of principal axes of strain-rate tensor in vicinity of terminus, showing arch of compression around a large embayment. Strain rate determined from average velocity for August 29 through November 8, 1977; terminus configuration is that on August 29, 1977.

arch of compression, and the maximum extension is normal to the border of the embayment. Perhaps this implies that calving is related to extension rate (R. L. Hooke, written commun., 1983) and that this arch (embayment) shape minimizes some aspect of the calving process. It is interesting that the large embayments formed in 1976–78 were buttressed on either side by portions of the glacier grounded on land or in shallow water and that there was little calving. Such possible buttressing points were much farther apart after 1978, and large embayments did not form.

By early summer, embayments have filled and the strain-rate field does not display such an obvious relation to terminus configuration. This condition also is evident in the strain-rate field averaged over the entire measurement year (pl. 7).

CONCLUSIONS

Over the past 25 years, the lower reach of Columbia Glacier has thinned and the terminus apparently has begun an irreversible retreat from the marine shoal against which it has rested since the first recorded observation nearly 200 years ago. Both the thinning and the retreat have accelerated in the past few years, and the pattern of thinning has slightly steepened the surface slope of the glacier's lower reach. In the summers of 1976–79, deep embayments were formed by high rates of calving localized in one segment or another of the glacier front; after 1980, retreat spread over most of the width of the terminus (pl. 4, fig. 10).

The spatial distribution of surface velocity is similar to that of an ice stream within an ice sheet because the speed in the main trunk of the glacier is much higher than in any of its tributaries. The speed exceeds 1 km/a both in the icefall reach and near the terminus (pl. 5). Extremely high strain rates occur in the icefall reach, ranging from 2.0 a^{-1} extension to 1.2 a^{-1} compression within about 1.3 km of each other, with a maximum strain-rate gradient of about 5×10^{-3} a^{-1} m^{-1}. The high longitudinal extension rate—along with a negligible transverse strain rate—indicates that, with typical mass-balance rates, the glacier must have extreme vertical strain rates in local areas.

The temporal variation of the lower reach velocity pattern (figs. 19–22) has three prominent characteris-

tics. The first characteristic is the amplitude of the annual variation, which along with the negligible annual variation of the surface topography indicates a high, seasonally varying sliding component of the motion. The second characteristic is the synchronism of the velocity change over most of the lower reach and the absence of any waves propagating downglacier. Both of these characteristics suggest the controlling influence of subglacial water. The third characteristic is the change in the velocity pattern near an embayment caused by rapid calving: the flow accelerates and turns inward, hastening the filling in of the embayment; the acceleration propagates upglacier and diffuses, and; an arch of compression forms in the velocity field (fig. 24) around the border of the embayment.

There is a fortunate correlation between a glacier's surface roughness and the efficacies of various observation methods. The highly fractured surface of Columbia Glacier (figs. 2, 3)—making even helicopter-assisted glacier travel extremely difficult and dangerous—is what provides the abundance of persistent, identifiable features necessary to photogrammetric analysis of high-altitude, vertical aerial photographs. Photogrammetry has the advantage of making it possible to process large volumes of data systematically. In addition, because photogrammetry is so highly mechanized and automated, the incidence of human error is significantly reduced. For the 6,634 individual points in this study of Columbia Glacier the error in coordinate determination is only about 3 m. Photogrammetry is fittingly complemented by the photograph-overlay method, which has an order-of-magnitude lower cost but an order-of-magnitude higher error.

There were several indications of the need for careful attention to analysis techniques. The painstaking application of the method of optimum interpolation was used because a popular, standard software module produced unsatisfactory results. Instead of using the poor approximation that the commonly used trajectory-average method would have provided, a differential equation was made to satisfy trajectory-endpoint conditions for determining the icefall velocity distribution. Because the thickness change measures only the sum of the mass balance and the emergence velocity, the two quantities cannot be determined separately by photogrammetry. The very large vertical strain rates likely to exist in the icefall would seriously impair the results of the conventional stratigraphic mass-balance method.

REFERENCES CITED

Adler, R. K. H., 1964, Some photogrammetric and geodetic aspects of measurement of glacier surface movement as a function of time: Journal of Glaciology, v. 5, no. 38, p. 229–234.

Bauer, Albert, 1968, Missions aeriennes de reconnaissance au Groenland 1957–58, *in* Expédition Glaciologique Internationale au Groenland (EGIG), 1957–60, v. 2, no. 3.

Bindschadler, R. A., 1983, The importance of pressurized subglacial water in separation and sliding at the glacier bed: Journal of Glaciology, v. 29, no. 101, p. 3–19.

Bindschadler, R. A., and Rasmussen, L. A., 1983, Finite-difference model predictions of the drastic retreat of Columbia Glacier, Alaska: U.S. Geological Survey Professional Paper 1258–D, p. 17.

Brecher, H. H., 1983, Photogrammetric determination of surface velocities and elevations on Byrd Glacier: Antarctic Journal of the United States, v. 17, no. 5, p. 79–81.

Brown, C. S., Meier, M. F., and Post, Austin, 1982, Calving speed of Alaska tidewater glaciers, with application to Columbia Glacier: U.S. Geological Survey Professional Paper 1258–C, 13 p.

Finsterwalder, Richard, 1931, Geschwindigkeitsmessungen an Gletschern mittels Photogrammetrie: Zeitschrift für Gletscherkunde, v. 19, no. 4–5, p. 251–262.

_____1938, Die geodätischen, gletsherkundlichen und geographischen Ergebnisse der deutschen Nanga Parbat Expedition 1934: Verlag Siegismund, Berlin.

Flammarion, Camille, 1880, Astronomie Populaire; revised by Gabriele Camille Flammarion and Andre Danjon, 1960: New York, Simon and Schuster, 670 p.

Fountain, A. G., 1982, Columbia Glacier photogrammetric altitude and velocity: data set (1957–1981): U.S. Geological Survey Open-File Report 82–756, 226 p.

Gandin, L. S., 1963, The objective analysis of meteorological fields: Leningrad, Hydrometeorological Publishing House. [English translation, Israel Program for Scientific Translations, Jerusalem, 1965, 242 p.]

Hodge, S. M., 1974, Variations in the sliding of a temperate glacier: Journal of Glaciology, v. 13, no. 69, p. 349–369.

Hofmann, Walther, 1952, Terrestrisch-photogrammetrische Gletschermessungen in den U.S.A.: Zeitschrift fur Vermessungswesen, 1953, no. 1, p. 16–21.

Iken, Almut, Röthlisberger, Hans, Flotron, A., and Haeberli, Wilfried 1983, The uplift of Unteraargletscher at the beginning of the melt season—A consequence of water storage at the bed?: Journal of Glaciology, v. 9, no. 101, p. 28–47.

Kniznikov, Yu. F., 1962, Obshchaya formula dlya opredeleniya poverkhostnoy skorosti dvizheniya I'da sposobom psevdoparallaksov [A general formula for the determination of the surface velocity of ice by the method of pseudoparallax]: Izvestiya Vysshikh Uchebnykh Zavedeniy. Geodizya i Aerofotos'yemka, v. 1, p. 61–65.

Lliboutry, Louis, and Reynaud, Louis, 1981, "Global dynamics" of a temperate valley glacier, Mer de Glace, and past velocities deduced from Forbes' bands: Journal of Glaciology, v. 27, no. 96, p. 207–226.

Mayo, L. R., Trabant, D. C., March, Rod, and Haeberli, Wilfried, 1979, Columbia Glacier stake location, mass balance, glacier surface altitude, and ice radar data, 1978 measurement year: U.S. Geological Survey Open-File Report 79–1168, 72 p.

Meier, M. F., Post, Austin, Brown, C. S., Frank, David, Hodge, S. M., Mayo, L. R., Rasmussen, L. A., Senear, E. A., Sikonia, W. G., Trabant, D. C., and Watts, R. D., 1978, Columbia Glacier progress report—December 1977: U.S. Geological Survey Open-File Report 78–264, 56 p.

Meier, M. F., Rasmussen, L. A., Post, Austin, Brown, C. S., Sikonia, W. G., Bindschadler, R. A., Mayo, L. R., and Trabant, D. C., 1980, Predicted timing of the disintegration of the lower reach of Columbia Glacier, Alaska: U.S. Geological Survey Open-File Report 80–582, 47 p.

Meier, Siegfried, 1973, Geodätische und glaziologischen Arbeiten am Hays-Gletscher Enderby-Land, Antarktis: Petermanns Geographische Mitteilungen, Gotha, v. 117, no. 1, 37 p.

Meier, Siegfried, Dressler, Klaus, Dietrich, R., Eger, R., 1978: Geodätisch-glaziologische Arbeiten am Hays-Gletscher, Enderby-Land, während der 17. Sowjetischen Antarktisexpedition 1972. Geodätische und Geophysikalische Veröffentlichungen, Nationalkommittee für Geodäsie und Geophysik der Deutsches Democratisches Republik, v. 3, no. 37.

Nye, J. F., 1952, The mechanics of glacier flow: Journal of Glaciology, v. 2, no. 12, p. 82–93.

_____1959, The deformation of the glacier below an ice fall: Journal of Glaciology, v. 3, p. 387–408.

_____1981, Structure and events in flow fields, *in* Balian, R., Kléman, M., Poirier, J. P., eds., Physique des defauts, Les Houches, session XXXV, 28 Juillet–29 Aout 1980: Amsterdam, North Holland, p. 551–568.

_____1983, Monstars on glaciers: Journal of Glaciology, v. 29, no. 101, p. 70–77.

Olsen, R. W., 1975, Simultaneous block adjustment of models: U.S. Geological Survey Computer Program H-276.

Paterson, W. S. B., 1981, The physics of glaciers: Oxford, Pergamon Press, 372 p.

Pillewizer, W., 1939, Die kartographischen und gletscherkundlichen Ergebnisse der deutschen Spitzbergen-Expedition, 1938: Petermanns Geographische Mittelungen. Ergänzungscheft, v. 238, 46 p.

Post, Austin, 1975, Preliminary hydrography and historical terminal changes of Columbia Glacier, Alaska: U.S. Geological Survey Hydrologic Investigations Atlas 559, 3 sheets.

Rasmussen, L. A., 1982, Quadratic spline subroutine package: U.S. Geological Survey Water-Resources Investigations 82–41, 16 p.

_____1983, Calculation of a velocity distribution from particle trajectory endpoints: Journal of Glaciology, v. 29, no. 102, p. 203–215.

Rasmussen, L. A., and Meier, M. F., 1982, Continuity equation model of the predicted drastic retreat of Columbia Glacier, Alaska: U.S. Geological Survey Profesisonal Paper 1258–A, 23 p.

Rasmussen, L. A., and Meier, M. F., 1984, Surface topography of the lower part of Columbia Glacier, Alaska, 1974–1981: U.S. Geological Survey Professional Paper 1258–E [in press].

Sikonia, W. G., 1982, Finite element glacier dynamics model applied to Columbia Glacier, Alaska: U.S. Geological Survey Professional Paper 1258–B, 74 p.

Sikonia, W. G., and Post, Austin, 1980, Columbia Glacier, Alaska: Recent ice loss and its relationship to seasonal terminal embayments, thinning, and glacier flow: U.S. Geological Survey Hydrologic Investigations Atlas 619, 3 sheets.

Slama, C. C., Theurer, Charles, and Henriksen, S. W., eds., 1980, Manual of photogrammetry (4th ed.): American Society of Photogrammetry Falls Church, Va., 1056 p.

Thorndike, A. S., Cooley, C. R., and Nye, J. F., 1978, The structure and evolution of flow fields and other vector fields: Journal of Physics, A: Mathematical and General, v. 11, no. 8, p. 1455–1490.

Vancouver, George, 1978, A voyage of discovery to the North Pacific Ocean and round the world in the years 1790–1795: London, printed for G. G. and J. Robinson, Paternoster-Row, and J. Edwards, Pall-Mall, v. 3.

Vickers, R. S., and Bollen, R., 1974, An experiment in the radio-echo sounding of temperate glaciers: Stanford Research Institute Project 3606, Final Report, Contract 14–08–0001–14650, 16 p.

Waddington, E. D., 1981, Accurate modeling of glacier flow: Vancouver, University of British Columbia, Department of Geophysics, Ph.D. dissertation, 460 p.

Weertman, Johannes, 1972, General theory of water flow at the base of a glacier or ice sheet: Reviews of Geophysics and Space Physics, v. 10, no. 1, p. 287–333.